VIRGINIA TECH
CENTER FOR ADHESION SCIENCE

CAS/ESM-86-4*
VPI-E-86.28

November 1986

NONLINEAR VISCOELASTIC ANALYSIS OF ADHESIVELY BONDED JOINTS
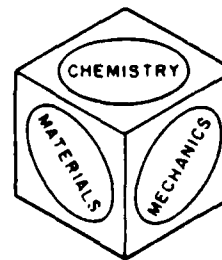
by

S. Roy and J. N. Reddy

Department of Engineering Science and Mechanics

DTIC
ELECTE
FEB 6 1987

A

VIRGINIA POLYTECHNIC INSTITUTE
AND STATE UNIVERSITY

216 NORRIS HALL
BLACKSBURG, VIRGINIA 24061

CHEMISTRY
MATERIALS
MECHANICS

Telephone: (703) 961-6824
TLX: EZLINK 9103331861
    VPI-BKS

...ved

87   2   6   050

NONLINEAR VISCOELASTIC ANALYSIS OF ADHESIVELY BONDED JOINTS

S. Roy and J. N. Reddy
Department of Engineering Science and Mechanics
Virginia Polytechnic Institute and State University
Blacksburg, VA 24061

November 1986

NONLINEAR VISCOELASTIC ANALYSIS OF ADHESIVELY BONDED JOINTS

S. Roy and J. N. Reddy
Department of Engineering Science and Mechanics
Virginia Polytechnic Institute and State University
Blacksburg, VA 24061

INTRODUCTION

Adhesive bonding is increasingly used to fasten structural components together. This is because in many present day applications, conventional fasteners such as bolts, rivets, welds etc., are unsuitable, specially if the components are made of polymeric or composite material. Penetration methods (i.e., drilling holes, etc.) cause high stress concentrations and, in the case of composites, sever the fiber reinforcement which in turn reduces the strength of the joint. On the other hand, bonded joints tend to be damage-tolerant due to the high damping behavior of the adhesive layer and less expensive due to lower fabrication cost.

Most polymeric adhesives are rate sensitive material and hence exhibit viscoelasticity. Furthermore, certain types of epoxy resins have been found to be nonlinearly viscoelastic in character. The nonlinear viscoelastic behavior is typified by a stress-enhanced creep. Basically, at elevated stresses the material moduli seem to soften and the creep progresses at accelerated rates.

At present there are numerous computer programs available for analyzing bonded joints. However, most of these computer codes incorporate linearly elastic material behavior, and some allow for nonlinearly elastic and plastic behavior. Computer programs which incorporate viscoelastic material behavior are quite often limited to the simple spring-dashpot type of model for linear materials. Such

1

inaccurate modelling of the constitutive behavior of the structure can seriously compromise the accuracy of the analytical predictions.

In this paper we are conerned with the development of a computational procedure which is capable of accurately modelling the linear and nonlinearly viscoelastic behavior of an adhesive layer within a bonded joint. The adherends can be modeled as a linearly elastic material which can undergo large rotations and displacements. The theory and computer implementation of the geometrically nonlinear elastic response has been presented in a previous work [1] and shall not be included here. The rest of the presentation will primarily involve the description and the implementation of a general constitutive law for nonlinear viscoelastic materials.

A general single integral constitutive law for nonlinear viscoelastic materials systems was proposed by Schapery [2]. The law can be derived from fundamental principles using the concepts of irreversible thermodynamics. A comprehensive review of the thermodynamics basis of Schapery's theory has been presented by Hiel et al. [3].

The present study deals with the development of a finite element model that is based on Schapery's single integral constitutive law. First, a stress operator that defines uniaxial strain as a function of current and past stress is developed. Extension to multi-axial stress state is accomplished by incorporating Poisson's effects, resulting in a constitutive matrix that consists of instantaneous compliance, Poisson's ratio and a vector of hereditary strains. The constitutive equation thus obtained are suitable for non-linear finite element analysis. Plane stress, plane strain and axisymmetric formulations are included.

2

A brief review of literature is presented in the next section to give the background for the present study.

BACKGROUND LITERATURE

An analysis of adhesive stresses in bonded joints was first performed by Goland and Reissner [4] for two limiting cases: (i) the case in which the adhesive layer is so thin and stiff that its deformation can be neglected; and (ii) the case in which the adhesive layer is soft and flexible and the joint flexibility is mainly due to the deformation of the adhesive layer. In the first case, the peel stress is found to be very high at the edge of the joint, while the shear stress is zero. In the second case, the maximum values of the peel and shear stresses occur at the edges of the joint. The Goland-Reissner analysis is limited to identical adherends, the joint-edge loads are not in equilibrium, and the stresses across the adhesive layer are constant.

Erdogan and Ratwani [5] developed a one-dimensional analytical model for calculating stresses in a stepped lap joint. One adherend was assumed to consist of an isotropic material and the second of an orthotropic material. Linear elastic conditions for the materials were assumed. The thickness variation of the stresses in both the adherends and in the adhesive was neglected.

Wooley and Carver [6] investigated the stress distributions in a simple lap joint using the finite element method. They assumed that the total length of the adherends beyond the overlap is long and a plane stress condition exists. The constant strain quadrilateral element (obtained by combining four constant strain triangular elements) was used. One end of the adherend was assumed to be hinged and other end

3

was allowed to move freely in the direction parallel to the original bond line. The study dealt with the influence of Young's moduli ratios and geometries on the peel and shear stress distributions. The results compared favorably with the results of Goland and Reissner.

Hart-Smith [7] improved upon the approach of Goland and Reissner by considering a third free-body-diagram for the adherend outside the joint in addition to the two free-body-diagrams from each of the upper and lower halves of the joint. With three separate sections to consider, three relations between displacements and bending moments were obtained. Additional boundary conditions involving displacements and their first derivatives, not considered by Goland and Reissner, were imposed in order to solve for the additional unknowns. In addition to the improvement on the analysis of Goland and Reissner, Hart-Smith [7] also estabished the quantitative influence of adhesive plasticity in shear. The elastic-plastic theory used by Hart-Smith predicts an increase in joint strength and was shown to be capable of explaining premature failure predictions found when using linear elastic analyses. The quantitative effects of stiffness imbalance were also accounted for.

A finite-element stress analysis for adhesive lap joints using linear elasticity and elasto-plasticity theories was reported by Liu [8]. Stress distributions and concentrations in the adhesive layer for different joint parameters (geometry, material properties, and loading conditions) were studied and compared.

The existence of stress gradients through the thickness of the adhesive layer, close to the joint edges, was observed by Adams and Peppiatt [9]. They subsequently performed a linear elastic finite

4

element analysis on adhesively bonded lap joints employing more than one element through the thickness of the adhesive layer, close to the joint edges. Adams and Peppiatt [10] also studied the adhesive yielding using an iterative elastic-plastic finite element program and the double lap, bevel and scarf joints. The adhesive was assumed to be elastic-perfectly plastic.

A nonlinear analysis of single and double lap joints was presented by Humphreys and Herakovich [11] using the finite element method. The nonlinear stress-strain response was represented by a Ramberg-Osgood approximation. Mechanical and thermal loadings were considered but only one element through the thickness of the adhesive layer was used.

Allman [12] presented an elastic stress analysis based on the strain energy density of a particular joint. The effects of bending, stretching and shearing of the adherends were included, and the shearing and tearing action in the adhesive was accounted for. All conditions of stress equilibrium in the joint and stress-free surface conditions were satisfied. It was assumed, however, that the axial stress varies linearly through the adherend thicknesses and that the shear stress is constant through the adhesive thickness. Allman obtained solutions for the single lap joint, although the method also appears to be applicable to other joint configurations. He found that the average shear stress concentration is 11% higher than that of Goland and Reissner's first analysis, while the average peel stress at the joint edge is 67% lower. Compared with the second analysis of Goland and Reissner, Allman's method yielded a shear stress concentration of 15% and 31% less for metal and composite adherends, respectively, while the average peel

5

stress at the joint edge was 27% higher and 36% lower for the same types of adherends, respectively.

Phenomenological considerations were discussed by Hart-Smith [13] which greatly improve our understanding of the sources of non-uniform load transfer, viz., adherend extensitivity, stiffness imbalance and thermal mismatch. He also explained how the lightly loaded central area of the joint, away from the joint edges, restricts cumulative creep damage, and suggests that this region is vital for long term durability. The amount of lightly loaded central area is a function of the overlap length.

Yuceoglu and Updike [14] developed a numerical method for determining peel and shear stresses in the adhesive of double lap, double strap and stiffner plate joints. Bending and transverse shear were included in the analytical model. Shear stresses were not required to drop to zero at the joint edges after reaching peak values close to the edges. Yuceoglu and Updike maintained that an analytical model which would allow the shear stresses to drop to zero at the joint edges would give approximately the same or slightly lower peak values of shear and peel stresses. Their method also reveals that adherend bending has a significant effect on both adhesive shear and peel stresses, especially the latter.

Delale and Erdogan [15,16] performed a plate analysis simiar to that of Goland and Reissner on the single lap joint assuming linear elastic adherends and a linear viscoelastic adhesive. Separate stress distributions were calculated for membrane loading, bending, and transverse shear loading. They further extended their viscoelastic

6

analysis of the single lap joint to include time-dependent temperature variations.

Gali and Ishai [17] performed a finite element analysis on a symmetric doubler model with linear elastic adherends and the adhesive obeying a nonlinear effective-stress-strain relationship. The effective-stress-strain relationship was derived from stress-strain curves obtained by tensile and shear test data, and based on the Von Mises deviatoric energy yield criterion. An iteration procedure was applied to the linearly elastic finite element problem using a specific secant modulus for each element separately. The secant modulus was found from the corresponding effective strain of the previous solution and the corresponding effective stress was found from the experimental stress-strain curves. Gali and Ishai analyzed the symmetric doubler model using both plane stress and plane strain and found that the plane strain solutions converged faster and yielded less conservative results (i.e., lower stresses) than the plane stress solutions. Nonlinear solutions were also found to be considerably lower than the linear solutions, the difference being more pronounced in the plane stress case. The problem was also solved with the adhesive following an elastic-perfectly-plastic effective-stress-strain law. The difference between these results and those of the continuous nonlinear effective-stress-strain case was found to be very small.

Nagaraja and Alwar [18] analyzed a tubular lap joint with the finite element method assuming linear elastic adherends and a nonlinear biaxial stress-strain law in the adhesive. They demonstrated that for low stress levels, of the order of 12% of the fracture stress, the nonlinear stresses were as much as 15% lower in shear and 8% lower in

peel than the linear stresses. Nagaraja and Alwar [19] also performed a finite element analysis on a single lap joint, treating the adherends as linear elastic materials but the adhesive as a linear viscoelastic material. The relaxation modulus was assumed to be equal to the inverse of the creep compliance, the latter being obtained experimentally.

Francis et al. [20] discussed the effects of a viscoelastic adhesive layer, geometry, mixed mode fracture response, mechanical load history, environmental history and processing variations on the fracture processes of adhesively bonded joints. However, their finite element analysis is based on linear elastic fracture mechanics.

Dattaguru, et al. [21] studied the crack lap specimen and performed analyses with a finite element program, GAMNAS, developed in-house at NASA-Langley. The program GAMNAS accounts for geometric and material nonlinearities but does not include viscoelastic capability. Also, fracture is modeled using the linear elastic fracture mechanics but no failure law is included.

Botha, Jones and Brinson [22], Henriksen [23], Becker, et al. [24], and Yadagiri and Papi Reddy [25] reported results of the viscoelastic, finite-element analysis of adhesive joints. Henriksen used Schapery's [2] nonlinear viscoelastic model to verify the experimental results of Peretz and Weitsman [26] for an adhesive layer. Becker et al. [24] developed a finite-element stress analysis program, called VISTA, for adhesively bonded joints. The program uses the nonlinear viscoelastic model of Knauss and Emri [27]. No illustrative or validation problems are presented to demonstrate the two-dimensional nonlinear viscoelastic capabilities of VISTA. The works of Botha, et al., and Yadagiri and Papi Reddy are limited to linear viscoelastic analysis.

8

Pickett and Hollaway [28] presented both classical and finite element solutions for elastic-plastic adhesive stress distributions in bonded lap joints. Single, double and tubular lap configurations having both similar and dissimilar adherends were considered. The results show how the development of adhesive yielding as the joints are loaded to a failure condition. The detrimental effect of adherend-stiffness-imbalance on the adhesive stress distributions was also shown.

An approximate method to analyze viscoelastic problems has been outlined by Schapery [29]. In this method, the solution to a viscoelastic problem is approximated by a corresonding elasticity solution wherein the elastic constants have been replaced by time dependent creep or relaxation functions. The method may be applied to linear as well as nonlinear problems. Weitsman [30] used Schapery's quasi-elastic approximation to investigate the effects of nonlinear viscoelasticity on load transfer in a symmetric double lap joint. Introducing a stress-dependent shift factor, he observed that the enhanced creep causes shear stress relief near the edges of the adhesive joint.

Schaffer and Adams [31] carried out a nonlinear viscoelastic analysis of a unidirectional composite laminate using the finite element method. The nonlinear viscoelastic constitutive law proposed by Schapery [2] was used in conjunction with elastoplastic constitutive relations to model the composite response beyond the elastic limit.

Ghoneim and Yu Chen [32] developed a viscoelastic-viscoplastic law based on the assumption that the total strain rate tensor can be decomposed into a viscoelastic and a viscoplastic component. A linear viscoelasticity model is used in conjunction with a modified plasticity

model in which hardening is assumed to be a function of viscoplastic strains as well as the total strain rate. The resulting finite element algorithm is then used to analyze the strain rate and pressure effects on the mechanical behavior of a viscoelastic-viscoplastic material.

Analysis of crack growth in viscoelastic media are mainly limited to linear isotropic, homogeneous materials. Schapery [33] proposed the use of parameters similar to the J integral for quasi-static crack growth in a class of nonlinear viscoelastic materials subject to finite strains.

Czarnocki and Piekarski [34] used a nonlinear elastic stress-strain law for three-dimensional failure analysis of a symmetric lap joint. Taking into account the variation of Poisson's ratio with strain within the adhesive, the authors concluded that the failure of the adhesive layer originates in the central plane of a joint (at the front edge). It was also observed that the joint width does not have any effect on the stress peaks in the central plane and that the application of a weaker but more flexible adhesive results in higher load carrying capacity and lower stress concentrations in the adherends.

NONLINEAR VISCOELASTIC FORMULATION

The uniaxial single integral constitutive equation can be stated as,

$$\epsilon(t) = g_0(t)\sigma(t)D_0 + g_1(t) \int_0^t D_c(\psi^t - \psi^s) \frac{d}{ds} [g_2(s)\sigma(s)]ds \quad (1)$$

In Eq. (1), $\epsilon(t)$ represents uniaxial kinematic strain at current time t, $\sigma(t)$ is the Cauchy stress at time t, D_0 is the elastic compliance and $D_c(\psi)$ is a transient creep compliance function. The factor $g_0(t)$ defines stress and temperature effects on elastic compliance and is a

measure of state dependent reduction (or increase) in stiffness.

Transient (or creep) compliance factor $g_1(t)$ has similar meaning,
operating on the creep compliance component. The factor $g_2(s)$ accounts
for the influence of load rate on creep, and depends on stress and
temperature. The functions ψ^t and ψ^s are reduced times at t and s,
respectively, and are defined by,

$$\psi^t = \int_0^t (a_{\sigma T}^s)^{-1} ds \tag{2}$$

where, $a_{\sigma T}^s$ is a time 'shift factor'. This function modifies
viscoelastic response as a function of temperature and stress.
Mathematically, $a_{\sigma T}^s$ shifts the creep data parallel to the time axis
relative to a master curve for creep strain versus time.

The constitutive law in Eq. (1) can be expressed in the following
operational form:

$$\varepsilon = F(\sigma) \tag{3}$$

where $F(\sigma)$ is a stress operator, defined by,

$$F(\sigma) = D_I \sigma + E \tag{4}$$

The detailed derivation of Eq. (4) from Eq. (1) is given below.

The transient creep compliance, $D_c(\psi)$, can be expressed in the
following exponential form,

$$D_c(\psi) = \sum_r D_r [1 - e^{-\lambda_r r^\psi}] \tag{5}$$

Substituting (5) in (1), gives,

$$\varepsilon = g_0 D_0 \sigma + g_1 \int_0^t \sum_r D_r [1 - e^{-\lambda_r (\psi^t - \psi^s)}] \frac{d}{ds} [g_2(s)\sigma(s)] ds \tag{6}$$

Letting the product $g_2 \sigma$ be expressed as G and simplifying the
integrand on the right hand side of Eq. (6) yields,

11

$$\epsilon = g_0 D_0 \sigma + g_1 \sum_r D_r \cdot \int_0^t \frac{d}{ds} G(s) ds - g_1 \sum_r D_r \cdot \int_0^t e^{-\lambda_r(\psi^t - \psi^s)} \frac{dG(s)}{ds} ds \tag{7}$$

The third integration term on the right hand side of Eq. (7) is now separated into two parts, the first part having limits from 0 to to $(t - \Delta t)$ and the second integral spanning only the current load step, i.e., from $(t - \Delta t)$ to t. Hence,

$$\int_0^t e^{-\lambda_r(\psi^t - \psi^s)} \frac{dG(s)}{ds} ds = \int_0^{t-\Delta t} e^{-\lambda_r(\psi^t - \psi^s)} \frac{dG(s)}{ds} ds$$

$$+ \int_{t-\Delta t}^t e^{-\lambda_r(\psi^t - \psi^s)} \frac{dG(s)}{ds} ds \tag{8}$$

Now, the first term on the right hand side of Eq. (8) can be rewritten as,

$$\int_0^{t-\Delta t} e^{-\lambda_r(\psi^t - \psi^s)} \frac{dG(s)}{ds} ds$$

$$= \int_0^{t-\Delta t} e^{-\lambda_r \psi^t} e^{\lambda_r \psi^s} \frac{dG(s)}{ds} ds$$

$$= \int_0^{t-\Delta t} e^{-\lambda_r \psi^t} e^{\lambda_r \psi^{t-\Delta t}} e^{\lambda_r \psi^s} e^{-\lambda_r \psi^{t-\Delta t}} \cdot \frac{dG(s)}{ds} ds$$

$$= \int_0^{t-\Delta t} e^{-\lambda_r(\psi^t - \psi^{t-\Delta t})} e^{-\lambda_r(\psi^{t-\Delta t} - \psi^s)} \frac{dG(s)}{ds} ds$$

$$= e^{-\lambda_r(\psi^t - \psi^{t-\Delta t})} \int_0^{t-\Delta t} e^{-\lambda_r(\psi^{t-\Delta t} - \psi^s)} \frac{dG(s)}{ds} ds$$

$$= e^{-\lambda_r \Delta \psi^t} q_r^{t-\Delta t} \tag{9}$$

where,

$$\Delta\psi^t = \psi^t - \psi^{t-\Delta t} \tag{10}$$

$$q_r^{t-\Delta t} = \int_0^{t-\Delta t} e^{-\lambda_r(\psi^{t-\Delta t}-\psi^s)} \frac{dG(s)}{ds} ds \tag{11}$$

The second integral on the right hand side of Eq. (8) is now integrated by parts. To carry out the integration, it is assumed that G varies linearly over the current time step Δt. Hence,

$$\int_{t-\Delta t}^t e^{-\lambda_r(\psi^t-\psi^s)} \frac{dG(s)}{ds} ds$$

$$= \frac{dG(s)}{ds} \left. \frac{e^{-\lambda_r(\psi^t-\psi^s)}}{\lambda_r} \right|_{t-\Delta t}^t - \int_{t-\Delta t}^t \frac{d^2G(s)}{ds^2} \frac{e^{-\lambda_r(\psi^t-\psi^s)}}{\lambda_r} ds$$

$$= \frac{dG(t)}{dt} \frac{1}{\lambda_r} - \frac{dG(t-\Delta t)}{dt} \frac{e^{-\lambda_r(\psi^t-\psi^{t-\Delta t})}}{\lambda_r}$$

$$= \frac{dG(t)}{dt} \left[\frac{1 - e^{-\lambda_r\Delta\psi^t}}{\lambda_r} \right] \tag{12}$$

In arriving at the second step, the fact that G(s) is assumed to be linear, hence its second derivative is zero, is used. Since G(t) has been assumed to be a linear function of time over the current load-step Δt, and the reduced time ψ is proportional to t, we can write,

$$\frac{dG(t)}{dt} = \frac{G(t) - G(t-\Delta t)}{\psi^t - \psi^{t-\Delta t}}$$

or,

$$\frac{dG(t)}{dt} = \frac{G(t) - G(t-\Delta t)}{\Delta\psi^t} \tag{13}$$

13

Substituting (13) into (12), gives,

$$\int_{t-\Delta t}^{t} e^{-\lambda_r(\psi^t - \psi^s)} \frac{dG}{ds} \, ds = [G(t) - G(t-\Delta t)][\frac{1 - e^{-\lambda_r \Delta \psi^t}}{\lambda_r \Delta \psi^t}]$$

or,

$$\int_{t-\Delta t}^{t} e^{-\lambda_r(\psi^t - \psi^s)} \frac{dG}{ds} \, ds = [G(t) - G(t-\Delta t)]\beta_r^t \qquad (14)$$

where

$$\beta_r^t = \frac{1 - e^{-\lambda \Delta \psi^t}}{\lambda_r \Delta \psi^t} \qquad (15)$$

Substituting (11) and (14) back into (7) and writing $G = g_2 \sigma$

$$\epsilon = g_0 D_0 \sigma + g_1 \sum_r D_r g_2 \sigma$$
$$- g_1 \sum_r D_r \{e^{-\lambda_r \Delta \psi^t} q_r^{t-\Delta t} + [g_2(t)\sigma(t) - g_2(t-\Delta t)\sigma(t-\Delta t)]\beta_r^t\} \quad (16)$$

Collecting those terms in Eq. (16) that are multiplied by current stress σ yields,

$$\epsilon = [g_0 D_0 + g_1 g_2 \sum_r D_r - g_1 g_2 \sum_r D_r \beta_r^t]\sigma$$
$$+ g_1 \{\sum_r D_r [g_2(t-\Delta t)\beta_r^t \sigma(t-\Delta t) - e^{-\lambda_r \Delta \psi^t} q_r^{t-\Delta t}]\} \qquad (17)$$

Defining instantaneous compliance D_I as the compliance term multiplying the instantaneous stress σ, and the remaining terms in Eq. (17) as hereditary strains E, yields,

$$\epsilon = D_I \sigma + E \qquad (18)$$

where,

$$D_I = g_0 D_0 + g_1 g_2 \sum_r D_r - g_1 g_2 \sum_r D_r \beta_r^t \qquad (19)$$

14

$$E = g_1\{\sum_r D_r[g_2(t-\Delta t)\beta_r^t\sigma(t-\Delta t) - e^{-\lambda_r\Delta\psi^t}q_r^{t-\Delta t}]\} \tag{20}$$

Hence, Eq. (18) expresses Schapery's single integral constitutive law in terms of a stress operator that includes instantaneous compliance and hereditary strains.

It is to be noted that the term $q_r^{t-\Delta t}$ in Eq. (20) is the rth component of the hereditary integral series at the end of the previous load step (i.e. at time equals $t - \Delta t$). The expression for the hereditary integral at the end of the current load step (i.e. at time t) can be derived in the form of a recurrence formula as shown below.

By definition [see. Eq. (11)],

$$q_r^t = \int_0^t e^{-\lambda_r(\psi^t-\psi^s)} \frac{dG}{ds} ds$$

$$= \int_0^{t-\Delta t} e^{-\lambda_r(\psi^t-\psi^s)} \frac{dG}{ds} ds + \int_{t-\Delta t}^t e^{-\lambda_r(\psi^t-\psi^s)} \frac{dG}{ds} ds$$

Using the results from Eqs. (11) and (14), the above equation reduces to,

$$q_r^t = e^{-\lambda_r\Delta\psi^t} q_r^{t-\Delta t} + [g_2(t)\sigma_{ij}(t) - g_2(t-\Delta t)\sigma(t-\Delta t)]\beta_r^t \tag{21}$$

where β_r^t is defined by Eq. (15).

MULTIAXIAL STRESS FORMULATION

As mentioned earlier, the constitutive law derived in the preceding section holds true for uniaxial state of stress. In order to formulate a stress strain relationship for a multiaxial stress state each strain component is assumed to be a linear function of the stress operators. Therefore, as in linear elastic analysis, Poisson's effect is

incorporated. Hence, the multiaxial stress strain law is fully defined
by the matrix relationship,

$$\{e\} = D_I[N]\{\sigma\} + [N]\{E\} \tag{22}$$

In Eq. (22), $\{e\}$ is a vector containing the algebraic difference of
kinematic strains $\{\epsilon\}$ and thermal strains $\{\delta_{ij}\theta\}$,

$$\{e\}^T = \{(\epsilon_{11} - \theta) \;,\; (\epsilon_{22} - \theta) \;,\; \gamma_{12} \;,\; (\epsilon_{33} - \theta)\} \tag{23}$$

while, $\{\sigma\}$ contains four components of Cauchy stress,

$$\{\sigma\}^T = \{\sigma_{11}, \sigma_{22}, \sigma_{12}, \sigma_{33}\} \tag{24}$$

and $\{E\}$ is a vector of hereditary strains, components of which are
defined by the equation,

$$\{E\}^T = \{E_{11}, E_{22}, E_{12}, E_{33}\} \tag{25}$$

Note that all quantities are functions of current time, t.

The matrix $[N]$ is a 4x4 matrix given by,

$$[N] = \begin{bmatrix} 1 & -\nu & 0 & -\nu \\ -\nu & 1 & 0 & -\nu \\ 0 & 0 & 2(1+\nu) & 0 \\ -\nu & -\nu & 0 & 1 \end{bmatrix} \tag{26}$$

where $\nu = \nu(t)$ is the Poisson's ratio at time t.

It is to be noted that the definitions (22) through (26)
incorporate possible states of plane stress, plane strain and rotational
symmetry.

16

Inversion of Eq. (22) gives a constitutive relationship which, written in a matrix form, is,

$$\{\sigma\} = [M]\{e\} - \frac{1}{D_I} \{E\} \qquad (27)$$

where [M] is,

$$[M] = \frac{1}{D_I(1+\nu)(1-2\nu)} \begin{bmatrix} 1-\nu & \nu & 0 & \nu \\ \nu & 1-\nu & 0 & \nu \\ 0 & 0 & (1-2\nu)/2 & 0 \\ \nu & \nu & 0 & 1-\nu \end{bmatrix} \qquad (28)$$

Equations (27) and (28) provide a general constitutive law and can be applied to either plane stress, plane strain or axisymmetric problems. For plane strain, kinematic strain component ε_{33} is identically zero. Hence, corresponding stresses may be computed by setting $\varepsilon_{33} = 0$. Since for plane stress, σ_{33} is identically zero, the kinematic strain ε_{33} can then be evaluated from Eq. (27) and (28) as,

$$\varepsilon_{33} = \frac{(1+\nu)(1-2\nu)}{(1-\nu^t)} E_{33} - \frac{\nu}{1-\nu}(\varepsilon_{11} - \theta) - \frac{\nu}{1-\nu}(\varepsilon_{22} - \theta) + \theta \qquad (29)$$

FINITE ELEMENT SOLUTION ALGORITHM

Basic Formulation

The principle of virtual work states that for a system to be in equilibrium (see [1,35]),

$$\delta W_{internal} = \delta W_{external}$$

or,
$$\delta W_{int} - \delta W_{ext} = 0 \qquad (30)$$

For any elastic structure,

$$\delta W_{int} = \int_V \sigma \delta \epsilon \, dv \tag{31}$$

where, $\delta \epsilon$ is the variation in the strain caused by the virtual displacement δu.

Equation (31) can be written in matrix form as,

$$\delta W_{int} = \int_V \{\delta \epsilon\}^T \{\sigma\} dv \tag{32}$$

The strain-displacement relations can be expressed as,

$$\{\delta \epsilon\} = [B]\{\delta u\} \tag{33}$$

where $[B]$ is the transformation matrix relating strains to displacements

$$[B] = \begin{bmatrix} \frac{\partial}{\partial x} & 0 \\ 0 & \frac{\partial}{\partial y} \\ \frac{\partial}{\partial y} & \frac{\partial}{\partial x} \end{bmatrix} \tag{34}$$

Needless to mention, the above relationship holds only for geometrically linear strain-displacement equations. Substituting Eq. (33) in Eq. (32) gives,

$$\delta W_{int} = \int_V \{\delta u\}^T [B]^T \{\sigma\} dv \tag{35}$$

The variation in external work due to virtual displacement $\{\delta u\}$ is given by,

$$\delta W_{ext} = \int_V \{\delta u\}^T \{F_{ext}\} dv \tag{36}$$

Substituting appropriate finite-element interpolation of the displacements (see [36]) into Eqs. (35) and (36), and substituting the result into Eq. (30), we obtain the finite-element equations,

$$\{\delta u\}^T \{ \int_V [B]^T \{\sigma^t\} dv - \{F_{ext}\}\} = \{0\} \tag{37}$$

18

where $\{\delta u\}$ is a vector of virtual displacements, and $\{F_{ext}\}$ is a vector of externally applied forces at the boundary.

If the stress vector $\{\sigma\}$ in Eq. (37) is now replaced by the multi-axial constitutive law, Eq. (27) derived previously, then Eq. (37) can be expanded as,

$$\{\delta u\}^T \{\int_V [B]^T[M]\{\epsilon\}dv - \int_V [B]^T[M]\{\theta\}dv$$

$$- \int_V \frac{1}{D_I} [B]^T\{E\}dv - \{F_{ext}\}\} = \{0\} \quad (38)$$

or simply,

$$\{\delta u\}^T\{R\} = \{0\}$$

where

$$\{R\} = \int_V [B]^T\{\sigma\}dv - \{F_{ext}\} \quad (40)$$

is the residual force vector.

Inspection of Eq. (36) reveals that it is a function of the instantaneous compliance D_I at the current time step. But from Eq. (19) it is observed that D_I is a function of g_0, g_1, g_2, and the reduced time and therefore dependent on the stress and temperature at the current time step. Hence, Eq. (38) is nonlinear and cannot be solved by the direct method. The solution must be obtained by means of an iterative method which is presented in the following section.

Iterative Scheme

In determining the solution to Eq. (38) at any time step t, the following approach is adopted. If $\{R_{i+1}\}$ is the vector of unbalanced forces at iteration i + 1 for time t, then,

$$\{R_{i+1}\} = \{R_i\} + [K_T]\{\Delta u_i\}$$

19

where $[K_T]$ is the tangent stiffness matrix,

$$[K_T] = \frac{d\{R\}}{d\{u\}} \tag{42}$$

in which $\{u\}$ is a vector of nodal displacements at time t. It can be shown from Eq. (38) that $[K_T]$ is given by,

$$[K_T] = \int_V [B]^T [M][B]dv \tag{43}$$

Since we seek for a solution in which $\{R_{i+1}\} = \{0\}$, incremental displacements $\{\Delta u_i\}$ are evaluated from,

$$\{\Delta u_i\} = - [K_T]^{-1}\{R_i\} \tag{44}$$

The displacement is updated after each iteration by,

$$\{u_{i+1}\} = \{u_i\} + \{\Delta u_i\} \tag{45}$$

As can be perceived, the above solution scheme is essentially the Newton-Raphson iterative solution algorithm.

Solution Algorithm

The complete solution procedure for each individual time step is presented in a logical step-wise fashion and can be used directly for programming purposes:

1. At the beginning of each time step, the stress vector $\{\sigma\}$ from the previous time step is accessed. Note that for the initial or starting time step, the stress vector $\sigma(t - \Delta t)$ denotes the initial stress state at $t = 0$, given by $\{\sigma^0\}$. Since it is customary to assume a stress free state

20

to exist at the start of the solution, $\{\sigma^0\}$ is usually set to be zero.

2. Temperature T at time t is computed from $T = f(t)$ which is supplied by the user for problems involving thermal loads.

3. The parameters $g_0(t)$, $g_1(t)$, $g_2(t)$, and $a_{\sigma T}^t$, which are known functions of temperature and stress, are evaluated next, using the stress vector obtained from previous load step.

4. Assuming $a_{\sigma T}^t$ to be a linear function of time over the time step Δt, the average value of shift factor is given as $a_{\sigma T_{avg}}^t = (a_{\sigma T}^{t-\Delta t} + a_{\sigma T}^t)/2$ and the change in reduced time $\Delta \psi^t$ is computed as $\Delta \psi^t = \Delta t / a_{\sigma T_{avg}}^t$. In order for this assumption to be valid Δt should be made sufficiently small.

5. Hereditary integral $\{q_r^t\}$ is computed using the recursive formula given by Eq. (21).

6. $\{F_{ext}\} = \lambda \{F_{app}\}$ where λ is the load factor that corresponds to the time step under consideration.

7. The residual vector $\{R\}$ is computed for each element as,

$$\{R\}^e = \{F_{ext}\}^e - \int_{v_e} [B]^T \{\sigma\}^e dv$$

8. The tangent stiffness matrix $[K_T]^e = \int_{v_e} [B]^T [M][B] dv$.

9. Incremental displacement $\{\Delta u\} = [K_T]^{-1}\{R\}$.

10. Total displacement $\{u\}_i = \{u\}_{i-1} + \{\Delta u\}_i$ where the subscript i denotes the number of iterations.

11. The strains and stresses are computed using the known displacement.

12. Steps 3 through 12 are repeated till $\dfrac{\|\{\Delta u_i\}\|}{\|\{u_i\}\|} <$ Tolerance.

21

13. Solution proceeds to the next time step for which steps 1

    through 12 are repeated.

SAMPLE PROBLEMS

Validation of Linear Viscoelastic Model

The nonlinear constitutive law due to Schapery may be linearized by assuming that the nonlinearizing parameters g_0, g_1, and g_2 have a value of unity. In addition, the stress dependent part of the exponent in the definition of the shift function is set to zero. Consequently, the constitutive law reduces to the hereditary integral form commonly used to describe a linear viscoelastic material.

Two test cases are used to validate the linear viscoelastic analysis capability implemented in the present finite element program named NOVA. In the first case, the tensile creep strain in a single eight noded quadrilateral element was computed for both the plane stress and plane strain cases using the program NOVA. The results were then compared to the analytical solution for the plane strain case presented in [37]. A uniform uniaxial tensile load of 13.79 MPa was applied on the test specimen. A three-parameter solid model was used to represent the tensile compliance of the adhesive. The Poisson's ratio was assumed to remain constant with time. The following time dependent functions were used in [37] (see [38] for additional experimental data on FM-73) to represent the tensile compliance and the Poisson's ratio for FM-73M at 72°C:

$$D(t) = \frac{G_0}{2[1+\nu(t)]} + \left\{\frac{G_1}{2[1+\nu(t)]}\right\}(1 - e^{-t/0.85})$$

$$\nu(t) = \frac{[\frac{3K(t)}{2G(t)} - 1]}{[\frac{3K(t)}{G(t)} + 1]},$$

where G(t) and K(t) are the shear and bulk modulus (mm/mm/MPA) respectively. The analytical solution to the creep problem for the plane strain case is given in [37] as:

$$\varepsilon(t) = 2.728 \times 10^{-2} + 1.334 \times 10^{-2} \, e^{-t/0.85} - 2.659 \times 10^{-4} \, e^{-t/0.3921}$$

It is to be noted that for the three-parameter solid characterization of FM-73M the value of the Poisson's ratio increases significantly with time. Consequently, the prony series coefficients for the tensile compliance also change with time. In the present formulation compliance coefficients are assumed to be independent of time. Hence two discrete values of the Poisson's ratio are used to match the exact solution for few initial time steps and final time steps. The values of the Poisson's ratio chosen for this purpose are $\nu_0 = \underset{t \to 0}{\text{Lim}} \, \nu(t) = 0.32$ and $\nu_\infty = \underset{t \to \infty}{\text{Lim}} \, \nu(t) = 0.417$. Figure 1a shows the creep curve for $\nu = 0.417$ for both plane strain and plane stress finite-element analyses. As expected, the plane strain results exhibit close agreement with the exact solution for large values of time, followed by progressive deterioration of predicted value as one moves towards smaller values of time. The finite element results for the plane stress case points to the fact that the strains are higher for plane stress than for plane strain.

Figure 1b shows the creep curve corresponding to $\nu = 0.32$. In this case the finite element predictions are accurate only for first few time steps and deviates more and more from the analytical solution as time increases. This is not surprising since the choice of Poisson's ratio for this case makes the comparison meaningful only when t is small.

The above results indicate that the program NOVA provides reasonably accurate results in regions where the input parameters are

23

accurate, and that the variation of Poisson's ratio during the period of analysis may cause significant deviations from the actual solution.

Next, the Model Joint analysis problem presented in [37] was used as the second validation example. In this case, a linear viscoelastic finite element analysis was carried out on a model joint under a constant applied load of 4448 N giving an average adhesive shear stress of 13.79 MPa. The specimen geometry, discretization and boundary conditions are shown in Fig. 2. The thickness of the adhesive layer is taken to be 0.254 mm. A nine parameter solid model was used to represent the tensile creep compliance of FM-73 at 72°C and is given by:

$$D(t) = 0.5988 \times 10^{-3} + 1.637 \times 10^{-5} (1 - e^{-t/0.01})$$

$$+ 0.6031 \times 10^{-4} (1 - e^{-t/0.1})$$

$$+ 0.9108 \times 10^{-4} (1 - e^{-t/1.0})$$

$$+ 2.6177 \times 10^{-4} (1 - e^{-t/10.0})$$

The Poisson's ratio is assumed to have a value of 0.417 and remains constant with time.

Figures 3 and 4 contain plots of the bond normal and shear stresses, respectively for t = 50 secs. and t = 60 min. of loading. These stresses represent the value at 1/16 the thickness from the upper adhesive adherend interface. The sharp peak at the left hand edge is due to the singularity caused by the presence of a re-entrant corner in the vicinity of the edge. These results are in good agreement with the results presented in [37] which uses the linear viscoelastic finite element code, MARC.

Validation of Nonlinear Viscoelastic Model

In order to validate the nonlinear viscoelastic model, three uniaxial test cases are analyzed. The results are compared with the laboratory tests conducted on similar specimens by Peretz and Weitsman [26]. The material properties used in the verification analysis are those reported in [23]. The creep data, together with other relevant material properties, are given in Table 1. A constant value for the Poisson ratio is assumed for the adhesive. The results from a linear viscoelastic analysis are also presented for comparison.

In the first verification test, a uniaxial stress of 10 MPa is applied to the adhesive coupon for 1200 secs., followed by a step increase to 26.6 MPa for a further 1200 secs. The temperature of the specimen is held constant at 50°C and is assumed to be uniform everywhere. The finite element predictions for this test are plotted together with the experimental data in Fig. 5. The predictions are in good agreement with the experimental results of Peretz and Weitsman [26].

The second test involves creep predictions under simultaneously varying stress and temperature, both increasing linearly with time. The temperature is again assumed to be uniform throughout the test specimen. The finite element predictions (linear and nonlinear) and experimental data are compared in Fig. 6. There is a good agreement between the two sets of data.

The third test involves creep under a constant stress of 10 MPa with a linearly varying temperature as a function of time. Figure 7 shows the strain vs. time curves obtained in the experiments and finite element analysis. Satisfactory agreement between the experimental results and the analysis is observed.

Stress Analysis of a Bonded Plate

After the successful validation of linear and nonlinear viscoelastic models, the program is used to investigate stresses and strains in a bonded cantilever plate undergoing bending due to a uniformly distributed transverse load (see in Fig. 8). The aluminum plates are bonded together by means of a thin layer of adhesive. The material properties used for aluminum are given in Table 2. The creep data used for the adhesive is the same as the one employed for the verification tests. The finite element mesh used for the problem is also shown in Fig. 8. A non-uniform mesh is used in anticipation of a large stress gradient near the clamped end. Eight-noded quadrilateral isoparametric plane strain elements are used for the analysis. The aluminum plates are assumed to be linearly elastic but undergoing large displacements, and the adhesive is assumed to be a nonlinearly viscoelastic material. Both the applied load and the temperature are assumed to be constant with time.

Figures 9 to 12 depict the results of this analysis over a period of 600 secs. Figure 9 contains plots of axial stresses, in aluminum and adhesive, plotted along the beam axis. Figures 10 and 11 contain the variation of the shear stresses and strains, respectively, along the axis of the beam. It can be seen that, the strains in the adhesive are an order of magnitude larger than the strains at a corresponding axial location in the aluminum. Furthermore, these strains increase in magnitude with an increase in time. While the stresses and strains within the aluminum plate (approximately) conform to the predictions of elementary beam theory, the corresponding strains and stresses within the adhesive layer exhibit significantly different behavior. The axial

stress within the adhesive change from compressive to tensile along the beam axis away from the clamped end. In the neighborhood of the free edge, the axial stress reaches a peak, followed by a sharp drop to zero at the free edge. The axial and shear stresses within the adhesive exhibit a certain amount of relaxation as time progresses.

Figure 12 shows through-the-thickness variation of the shear stress at two different locations, x = 13 mm and 89 mm, along the beam axis. The area under each curve is obtained by means of numerical integration to verify the equilibrium. The total vertical force at each section did not change with time and was reasonably close to the actual applied force in the transverse direction. It is clear from the results that the adhesive layer experiences the largest shear stress close to the free end than near the clamped end.

Linear and Nonlinear Analysis of a Model Joint:

The loading, boundary conditions and specimen geomtry used in this analysis is the same as the one used in the earlier model joint (see Fig. 1). In addition, the same nine parameter solid model was used in this analysis. A linear viscoelastic finite element analysis was carried out over a period of one hour at a constant applied load of 3336 N. The results for the linear analysis are shown in Figs. 13-14. The sharp peak at the left hand edge is due to the singularity caused by the presence of a re-entrant corner. All stress plots show the same basic trend in that the stresses are attempting to redistribute themselves to achieve a more uniform distribution.

For the nonlinear viscoelastic analysis of the model joint, the same specimen geometry and material properties were employed. However, the nonlinearizing parameters and the shift function were no longer held

constant, but were allowed to change with the current stress state within the adhesive layer. The results from this analysis are presented in Figs. 15-16. It is immediately apparent that the effect of the nonlinearity causes a 'softening' of the adhesive, leading to a response that is less stiff compared to the linear case. Hence, even though the applied load is the same, the shearing strain for the nonlinear case is significantly larger as compared to the linear case (Figs. 14 and 16). Moreover, the increment in creep strain for the nonlinear case is 0.0058 as compared to 0.0041 for the linear case over the same period of time. This is exactly what is expected since the nonlinear model takes into account the acceleration of creep caused by the stresses within the adhesive.

The effect of the nonlinearity on the stress curves (Figs. 13 and 15) is to create a more uniform stress distribution by reducing the stress peaks near the edges while increasing the stresses at the mid-section of the overlap. The significant reduction of the stress peaks effected by the nonlinear model is very important from a design point of view since the reduction of stress levels at the critically stressed regions results in an improved joint efficiency.

Stress Analysis of a Thick Adherend Lap Shear Specimen

The geometry, boundary conditions and finite element mesh of the thick adherend lap shear specimen are shown in Fig. 17. The load and the temperature are kept constant with time. The material used for the adherend is aluminum, and the adhesive is FM-73. The properties of these materials have been 1. ted in Tables 1 and 2. The aluminum is assumed to be linearly elastic and the adhesive is nonlinearly viscoelastic.

28

The analysis is carried out for a time period of 1200 secs. The results are shown in Figs. 18-21. At the free edge corresponding to x/c = -1, there appears to be the same kind of relaxation mechanism at work since the stresses at that location tend to decrease with time. Almost all stresses and strains exhibit a sharp peak at x/c = 1, and this peak becomes more dominant with time. The re-entrant corner and the associated singularity in the vicinity of the right hand edge is the cause for this unsymmetric behavior.

At the center of the bond, the axial and peel strains do not change appreciably with time. The shear strain on the other hand increases by 24% over the first 600 secs. followed by a further increase of 4% over the next 600 secs. Hence the shear strain increases asymptotically with time under a constant shear stress, which is typical for a viscoelastic material. Numerical integration of the areas under the shear stress plot at each time step yielded the same value for the total shear force to within 0.5% accuracy. A plot of the axial displacement of points along the lower bondline at different time steps is shown in Fig. 21. The displacement of the upper bondline, shown at the bottom of the figure, does not change with time. The average shear strain at any point along the bond is given by the difference in the axial displacement between upper and lower bondline divided by the distance separating the two bondlines. The values of the average shearing strain obtained from the displacement plot are in good agreement with the results displayed in the strain plot.

The stress relaxation mechanism near the free edge is not very effective at the right hand edge due to the presence of the aforementioend singularity which causes the stresses to increase with

time. This is certainly true for the relatively short time span under consideration. The durability of the bond over longer time spans is likely to depend upon which one of these two effects dominate.

Stress Analysis of a General Scarf Joint

The last example deals with the stress analysis of a scarf joint (see Fig. 22a). The adhesive is FM-73 while the adherends are of aluminum. The analysis is restricted to a constant load over a period of 900 sec. under isothermal conditions. The finite element meshes used in these analyses for $\alpha = 0^\circ$ and $\alpha = 45^\circ$ are shown in Figs. 22b and c, respectively.

The results for the butt joint (i.e. $\alpha = 0^\circ$) are shown in Figs. 23 and 24. Stresses and strains are plotted along with the width of the joint for the adhesive and the adherend. The stresses in the adhesive normal to the bondline are the same as those in the adherend and their magnitudes remain constant with time. Hence axial equilibrium is satisfied at all times. On the other hand, the normal strain in the adhesive is two orders of magnitude higher than that in the aluminum, and it shows a 21% increase in magnitude over the selected time span. Such large normal strain in the adhesive gives rise to fairly large tensile stress in the transverse direction, even though the transverse strain is negative. The shear stresses and strains are zero everywhere within the butt joint, except near the free edge.

The results for the scarf joint, for $\alpha = 45^\circ$, are shown in Figs. 25 and 26. The normal and transverse stresses follow a pattern similar to the stresses in a butt joint. The reduction in the magnitude of these stresses is due to the 45° inclination of the bond to the load direction. The most notable difference between the results of the butt

joint and the scarf joint is that the shear stresses and strains in the scarf joint have large positive values within the adhesive. In fact, the shear stress is equal in magnitude to the normal stress while the shear strain is an order of magnitude larger than the normal strain. The normal strain for the scarf joint increases by 38% over 900 seconds, while the shear strain increases by 16% over the same period of time.

The large shear stress present in the scarf bond over a period of time, causes the adherends to slide past one another. Hence, while it may be advantageous to use a scarf joint over a butt joint due to reduced stress levels, long term loading of a scarf joint may lead to serious misalignment due to bending of the adherends.

SUMMARY AND CONCLUSIONS

A nonlinear viscoelastic computational model is developed, validated and applied to the stress analysis of adhesively bonded joints. The nonlinear viscoelastic model used is that of Schapery. The finite element formulation is based on the updated, incremental Lagrangian formulation. The program is validated by comparing the present results with available analytical and experimental results. Additional results for bonded cantilever plate, thick adherend specimen and scarf joint are also presented. In general, the computer program developed herein, called NOVA, is believed to provide accurate nonlinear viscoelastic analysis capability.

The program will be further generalized to account for laminated composite (or anisotropic) adherends, moisture effects, and crack initiation and growth in nonlinear viscoelastic media in our future work.

31

REFERENCES

1. J. N. Reddy and S. Roy, "Finite Element Analysis of Adhesively Bonded Joints," Report No. VPI-E-85.18, Department of Engineering Science and Mechanics, VPI&SU, Blacksburg, VA 1985.

2. R. A. Schapery, "Further Development of a Thermodynamic Constitutive Theory: Stress Formulation," A&S Report No. 69-2, Purdue University, W. Lafyette, Feb. 1969.

3. C. Hiel, A. H. Cardon, and H. F. Brinson, "The Nonlinear Viscoelastic Response of Resin Matrix Composite Laminates," Report VPI-E-83-6, Department of Engineering Science and Mechanics, Virginia Polytechnic Institute and State University, Blacksburg, VA, March 1983.

4. M. Goland and E. Reissner. "The Stresses in Cemented Joints," Applied Mechanics, Vol. 1, pp. A17-A27, March 1944.

5. F. Erdogan and M. Ratwani, "Stress Distributions in Bonded Joints," Composite Materials, Vol. 5, pp. 378-393, 1971.

6. G. R. Wooley and D. R. Carver, "Stress Concentration Factors for Bonded Lap Joints," J. Aircraft, Vol. 8, No. 10, pp. 817-820, 1971.

7. L. J. Hart-Smith, "Adhesive Bonded Single Lap Joints," NASA CR-112236, January 1973.

8. A. T. Liu, "Linear Elastic and Elasto-Plastic Stress Analysis for Adhesive Lap Joints," T.A.M. Report No. 410, University of Illinois at Urbana-Champaign, July 1976.

9. R. D. Adams and N. A. Peppiatt, "Stress Analysis of Adhesively Bonded Lap Joints," Strain Analysis, Vol. 9, No. 3, pp. 185-196, 1974.

10. R. D. Adams and N. A. Peppiatt, "Stress Analysis of Lap Joints in Fibre Reinforced Composite Materials," Fibre Reinforced Plastics, London, ICE, p. 45, 1977.

11. E. A. Humphreys and C. T. Herakovich, "Nonlinear Analysis of Bonded Joints with Thermal Effects," Report VPI-E-77.19, Department of Engineering Science and Mechanics, Virginia Polytechnic Institute and State University, Blacksburg, Virginia, May 1977.

12. D. J. Allman, "A Theory for Elastic Stresses in Adhesive Bonded Lap Joints," Mechanics and Applied Mathematics, Vol. 30, 4, pp. 415-436, November 1977.

13. L. J. Hart-Smith, "Analysis and Design of Advanced Composite Bonded Joints," NASA CR-2218, April 1974.

14. U. Yuceoglu and D. P. Updike, "Stress Analysis in Bonded Plates and Joints," Engineering Mechanics Division, ASCE, Vol. 106, pp. 37-56, 1980.

15. F. Delale and F. Erdogan, "Viscoelastic Analysis of Adhesively Bonded Joint," J. Appl. Mechanics, Vol. 48, pp. 331-338, 1981.

16. F. Delale and F. Erdogan, "Time Temperature Effect in Adhesively Bonded Joints," J. Composite Materials, Vol. 5, pp. 561-581, 1981.

17. S. Gali and O. Ishai, "Interlaminar Stress Distribution Within an Adhesive Layer in the Non-linear Range," Journal of Adhesion, Vol. 9, pp. 253-266, October 1978.

18. Y. R. Nagaraja and R. S. Alwar, "Nonlinear Stress Analysis of an Adhesive Tabular Lap Joint," Journal of Adhesion, Vol. 10, No. 2, pp. 97-106, 1979.

19. Y. R. Nagaraja and R. S. Alwar, "Viscoelastic Analysis of an Adhesive-Bonded Plane Lap Joint," Computers and Structures, V11, 6, pp. 621-627, 1980.

20. E. C. Francis, W. L. Hufferd, D. G. Lemini, R. E. Thompson, W. E. Briggs and R. R. Parmerter, "Time Dependent Fracture in Adhesive Bonded Joints," Chemical Systems Division, Sunnyvale, California, Interim Reports CSD 2769-1R-01/02, May and Nov. 1982.

21. B. Dattaguru, R. A. Everette, Jr., J. D. Whitcomb, and W. S. Johnson, "Geometrically Nonlinear Analysis of Adhesively Bonded Joints," J. Engng. Materials and Technology, Vol. 106, pp. 59-65, 1984.

22. L. R. Botha, R. M. Jones, and H. F. Brinson, "Viscoelastic Analysis of Adhesive Stresses in Bonded Joints," Report VPI-E-83-17, May 1983, Virginia Polytechnic Institute, Blacksburg, VA.

23. M. Henriksen, "Nonlinear Viscoelastic Stress Analysis - A Finite Element Approach," Computers and Structures, Vol. 18, No. 1, pp. 133-139, 1984.

24. E. B. Becker et al., "Viscoelastic Stress Analysis Including Moisture Diffusion for Adhesively Bonded Joints," AFWAL-TR-84-4057, General Dynamics, Ft. Worth Division, TX, August, 1984.

25. S. Yadagiri and C. Papi Reddy, "Viscoelastic Analysis of Nearly Incompressible Solids," Computers and Structures, Vol. 20, No. 5, pp. 817-825, 1985.

26. D. Peretz and Y. Weitsman, "The Non-Linear Thermo-Viscoelastic Characterizations of FM-73 Adhesives,," J. Rheology, Vol. 26, pp. 245-261, 1983.

27. W. G. Knauss and I. J. Emri, "Nonlinear Viscoelasticity Based on Free Volume Considerations," Computers and Structures, Vol. 13, pp. 123-128, 1981.

28. A. K. Prickett and L. Hollaway, "The Analysis of Elastic-Plastic Adhesive Stress in Bonded Lap Joints in FRP Structures," Composite Structures, Vol. 4, pp. 135-160, 1985.

29. R. A. Schapery, "A Method of Viscoelastic Stress Analysis Using Elastic Solutions," Journal of the Franklin Institute, Vol. 279, pp. 268-289, 1965.

30. Y. Weitsman, "An Investigation of Non-Linear Viscoelastic Effects on Load Transfer in a Symmetric Double Lap Joint," J. Adhesion, Vol. 11, pp. 279-289, 1981.

31. B. G. Schaffer and D. F. Adams, "Non-Linear Viscoelastic Analysis of a Unidirectional Composite Material," J. Appl. Mech., Vol. 48, p. 859, 1981.

32. H. Ghoneim and Y. Chen, "A Viscoelastic-Viscoplastic Constitutive Equation and its Finite Element Implementation," Computers and Structures, Vol. 17, No. 4, pp. 499-509, 1983.

33. R. A. Schapery, "Correspondence Principles and a Generalized J Integral for Large Deformation and Fracture Analysis of Viscoelastic Media," International Journal of Fracture, Vol. 25, pp. 195-223, 1984.

34. P. Czarnocki and K. Piekarski, "Nonlinear Numerical Stress Analysis of a Symmetric Adhesively Bonded Lap Joint," International Journal of Adhesion and Adhesives, Vol. 6, No. 3, July 1986.

35. J. N. Reddy, Energy and Variational Methods in Applied Mechanics, Wiley, New York, 1984.

36. J. N. Reddy, An Introduction to the Finite Element Method, McGraw-Hill, New York, 1984.

37. Quarterly Progress Report No. 6 (1 Dec. 1980 to 23 Feb. 1981), "Integrated Methodology for Adhesive Bonded Joint Life Predictions," General Dynamics,Fort Worth Division,Technical Report FZM-6961, March 1981.

38. M. A. Rocheport and H. F. Brinson, "Nonlinear Viscoelastic Characterization of Structural Adhesives," Report VPI-E-83.26, Department of Engineering Science and Mechanics, Virginia Polytechnic Institute and State University, Blacksburg, VA, July 1983.

TABLE 1

Material Data for FM-73 Unscrimmed
(At Ref. Temp. 303°K)

Elastic Compliance, D_o: 360×10^{-6}/MPa

Creep Compliance, D_c: 29×10^{-6}/MPa

Power Law Exponent, n: 0.12

Poisson's Ratio, ν: 0.38

Coefficient of Thermal Expansion, α: 6.6×10^{-5} m/m/°K

Table 2

Material Data for Aluminum

Young's Modulus, E_1: 70×10^3 MPa

Poisson's Ratio, ν: 0.34

Coefficient of Thermal Expansion, α: 7.17×10^{-6} m/m/°K
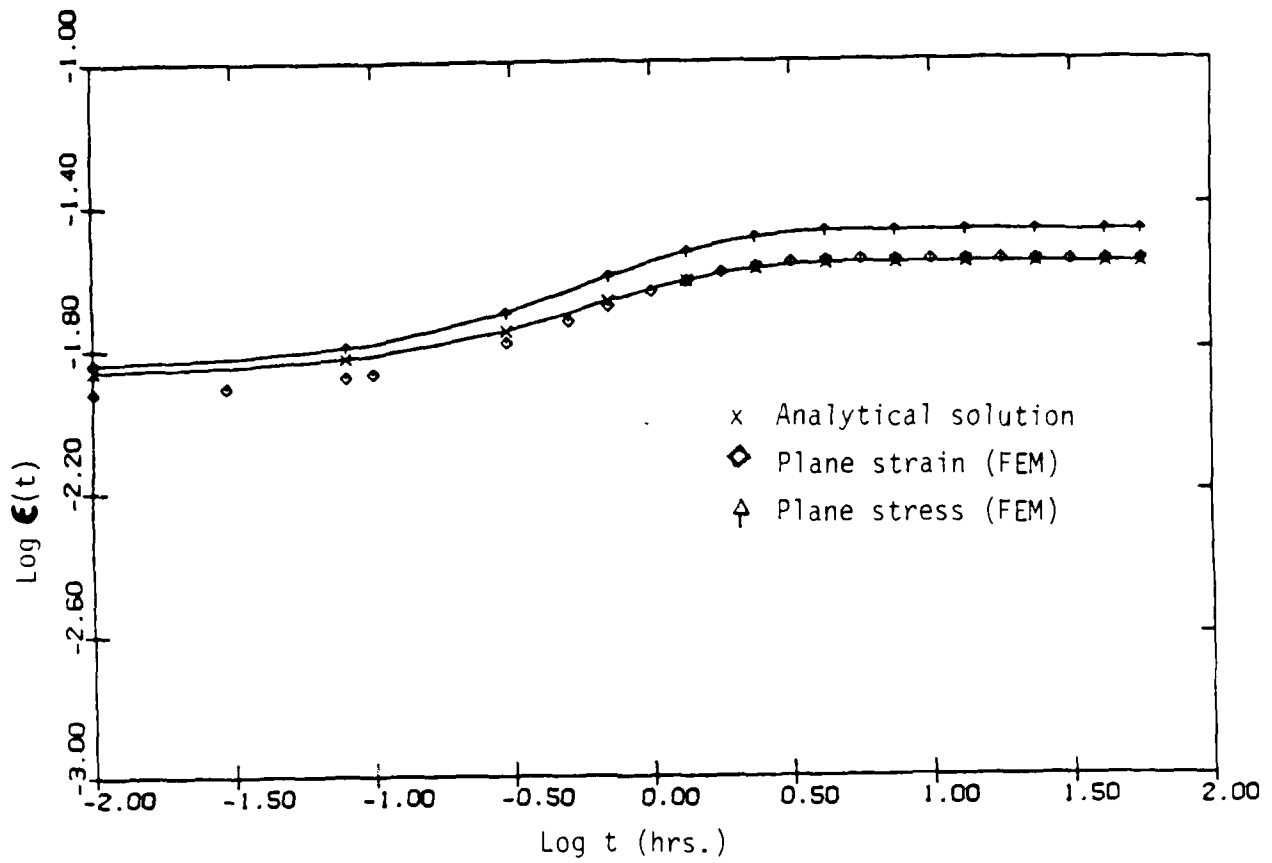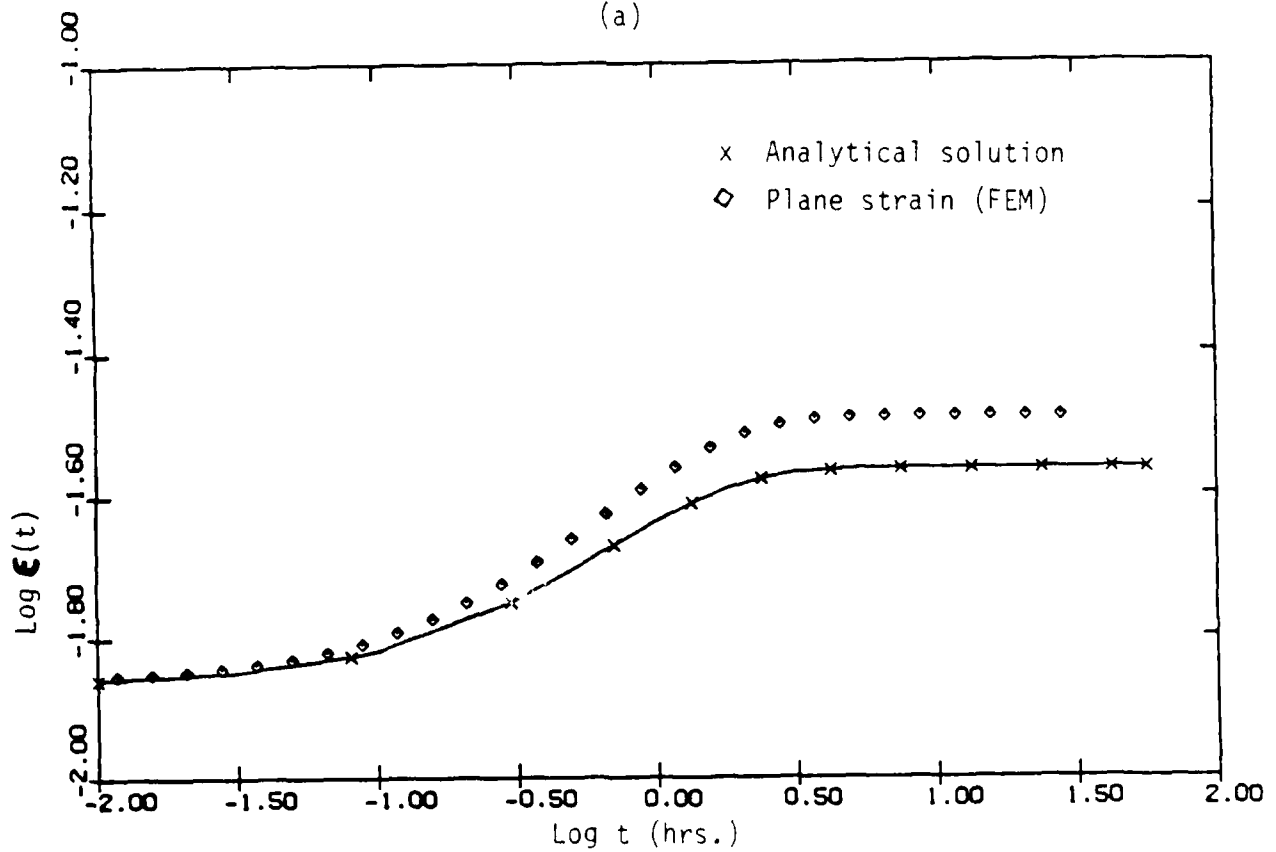
Fig. 1 Comparison of the finite element solution with analytical solution of a linear viscoelastic coupon characterized by three-parameter solid.
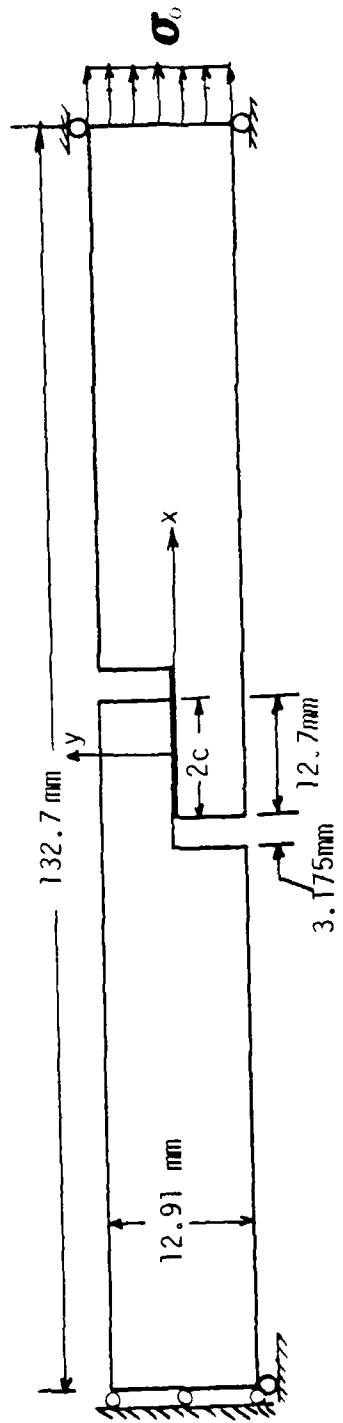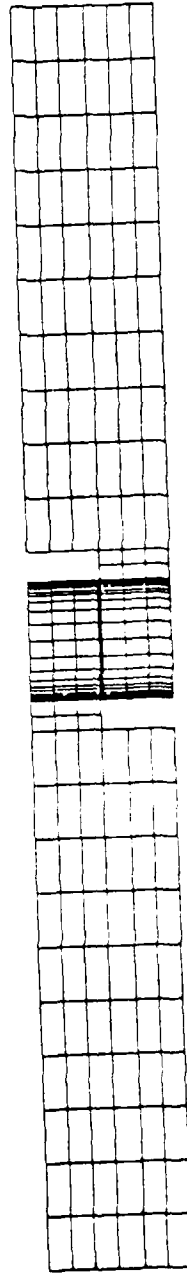
Fig. 2   The geometry, boundary conditions, loading and finite element mesh used for the model joint problem.
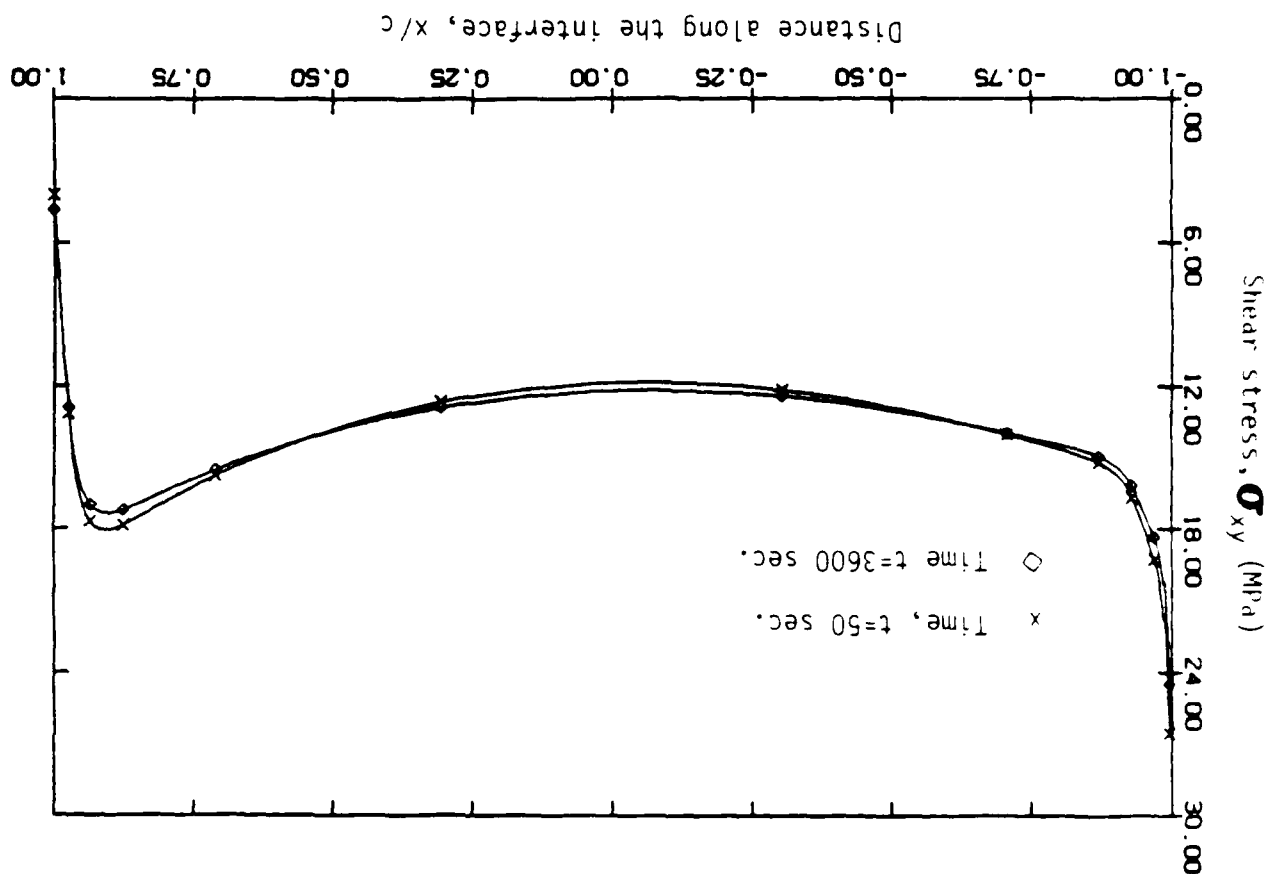
(a)

(b)

132.7 mm

12.91 mm

12.7mm

3.175mm

2c

σ_o

x

y
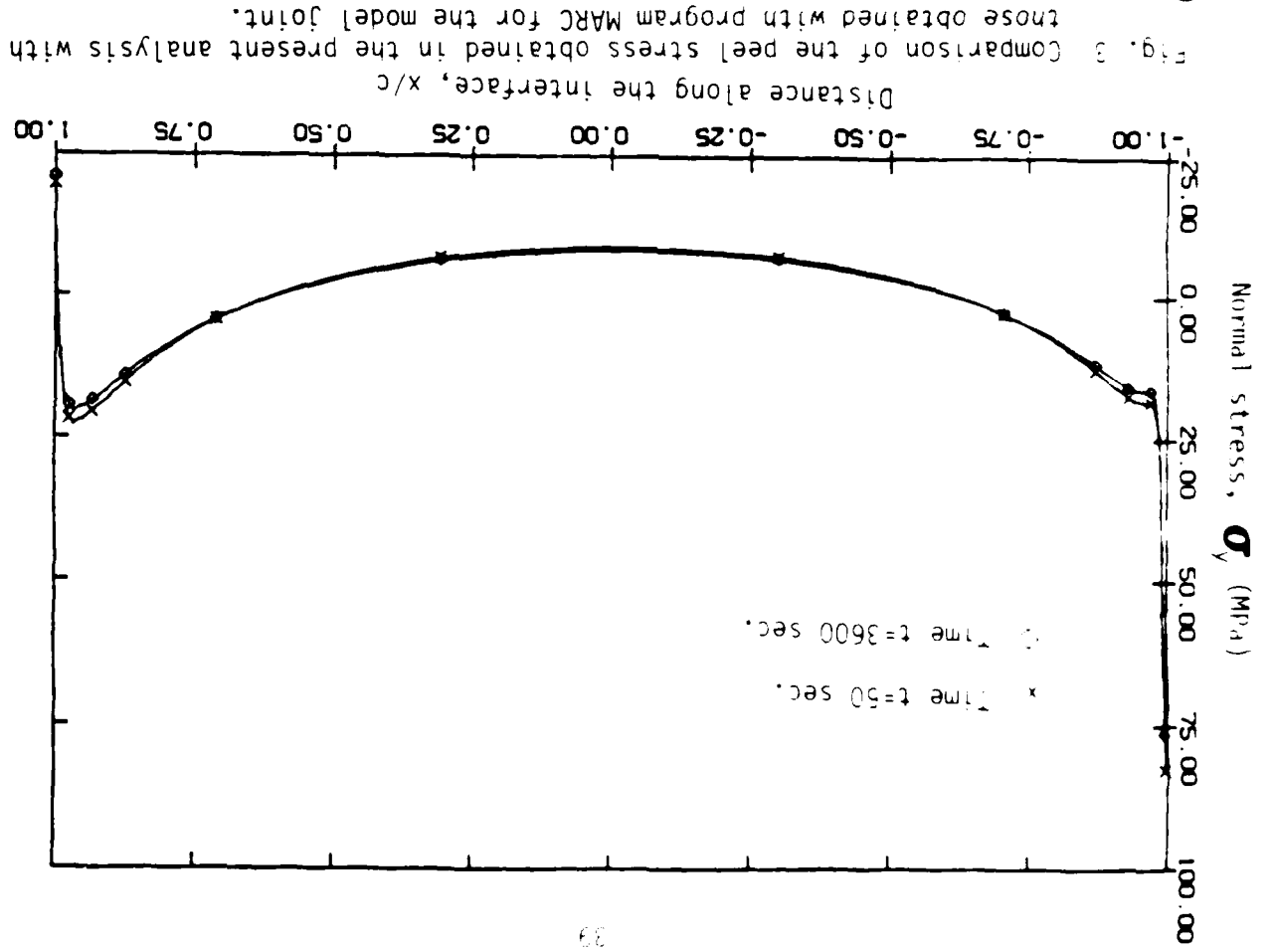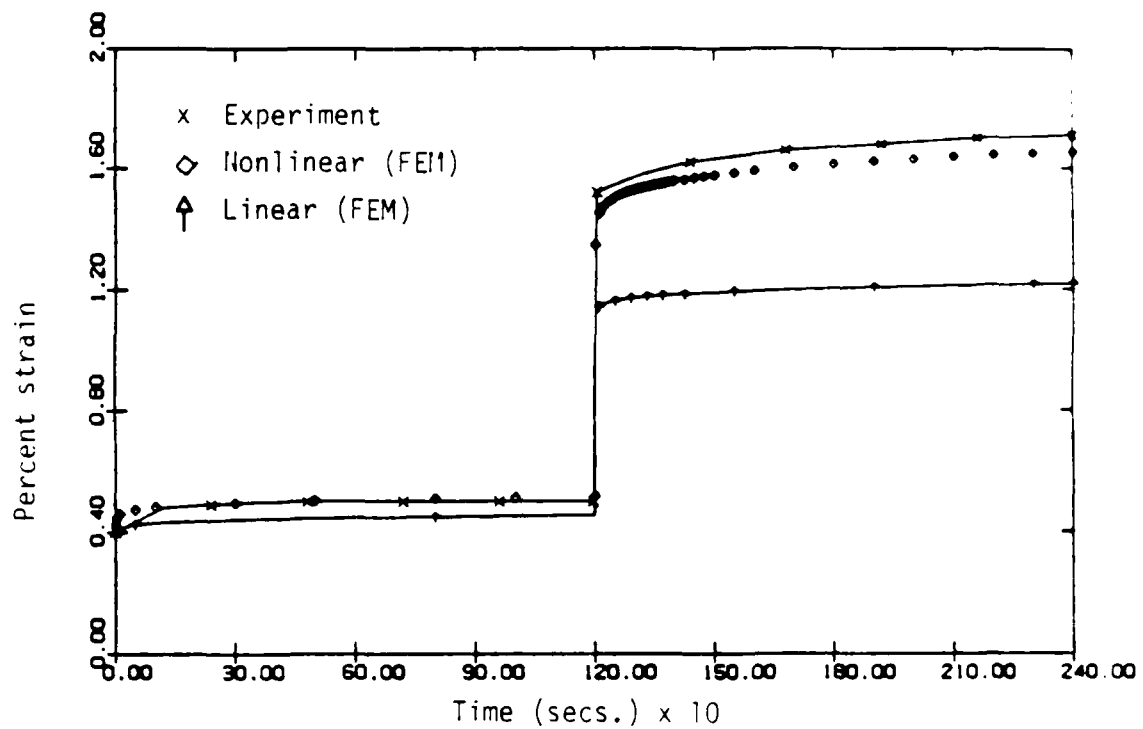
Fig. 5 Strain versus time for FM-73 adhesive for step loading at constant temperature.
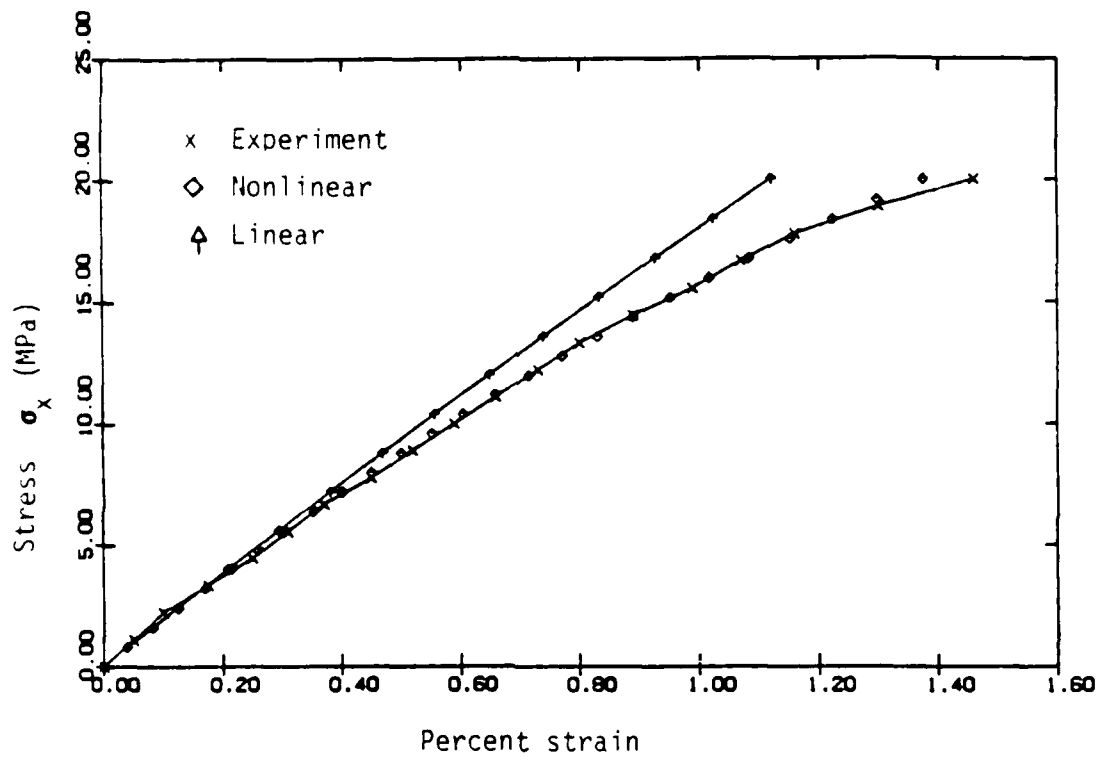
Fig. 6 Stress versus strain for FM-73 adhesive layer under linear temperature and stress.
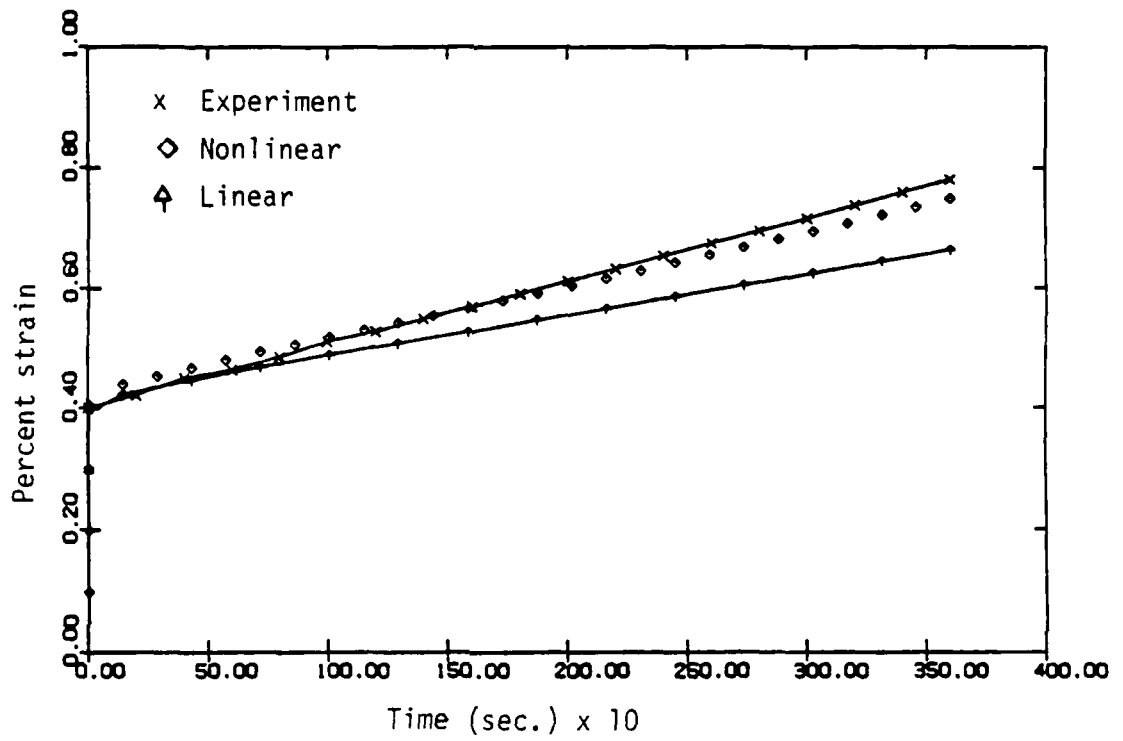
Fig. 7 Stress versus strain for FM-73 adhesive layer under linear temperature and constant stress.
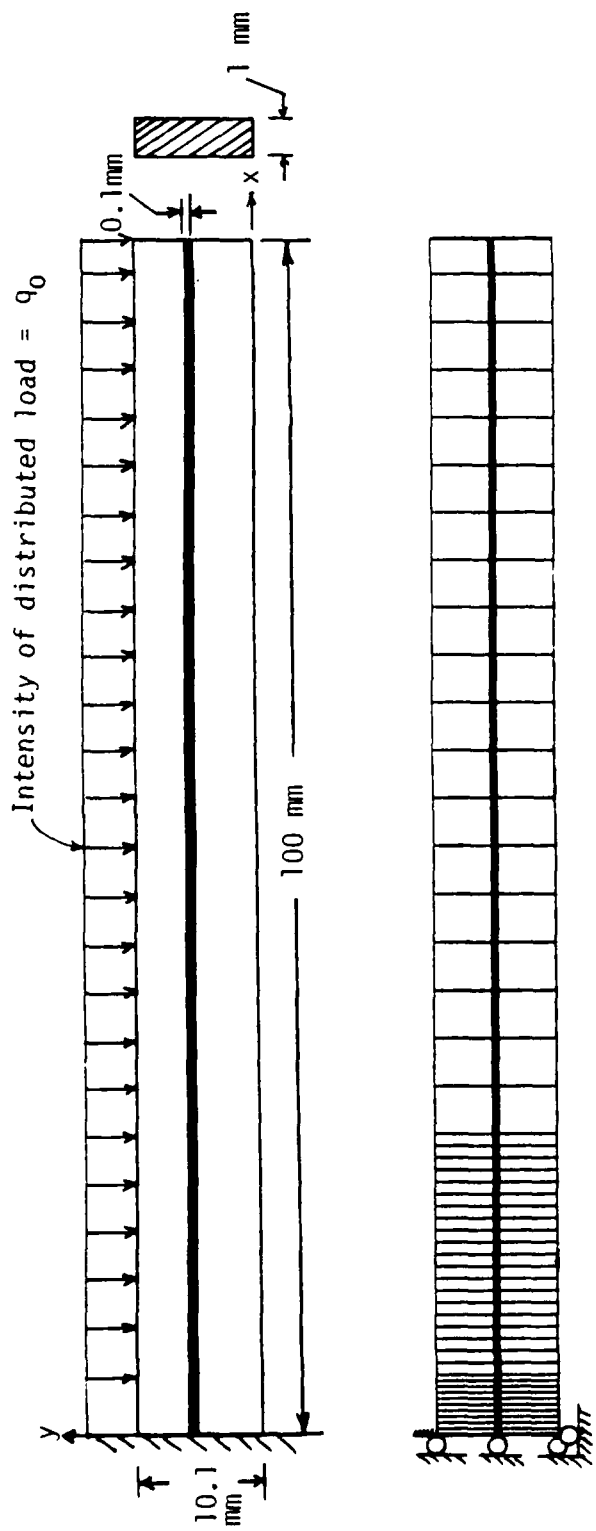
Fig. 8 Geometry, loading and finite element mesh used in the bonded cantilever plate problem.
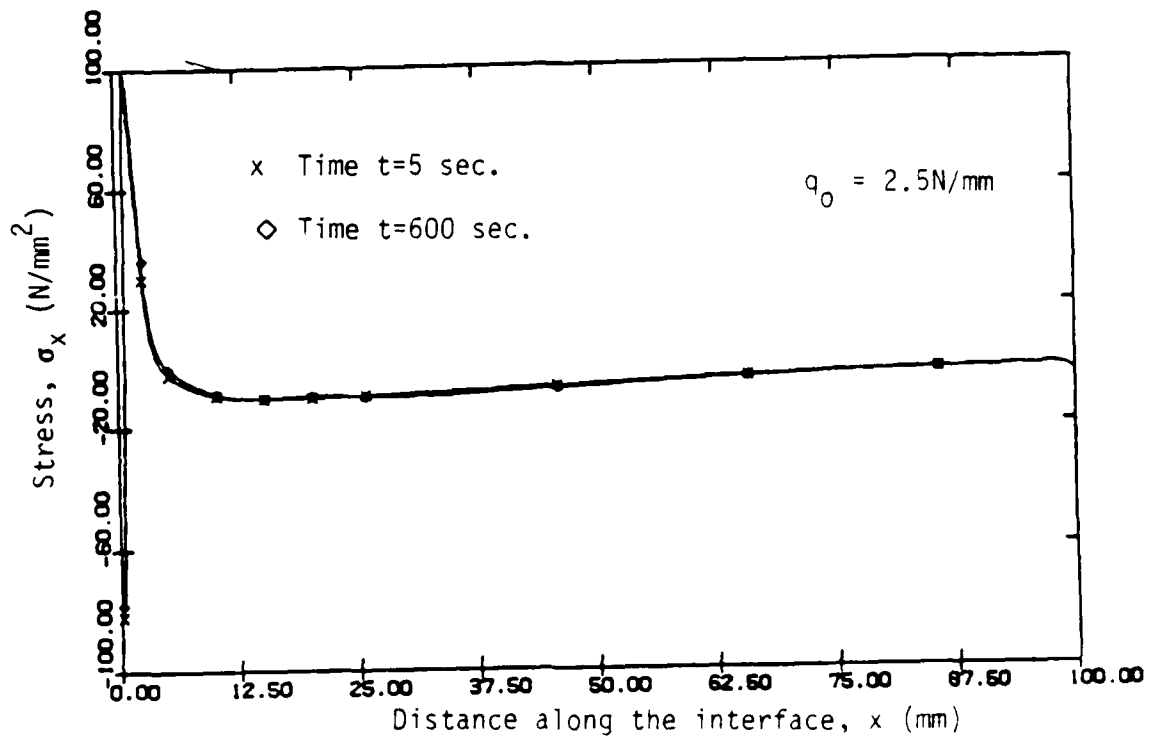
(a) Axial stress in aluminum at y=4.96mm
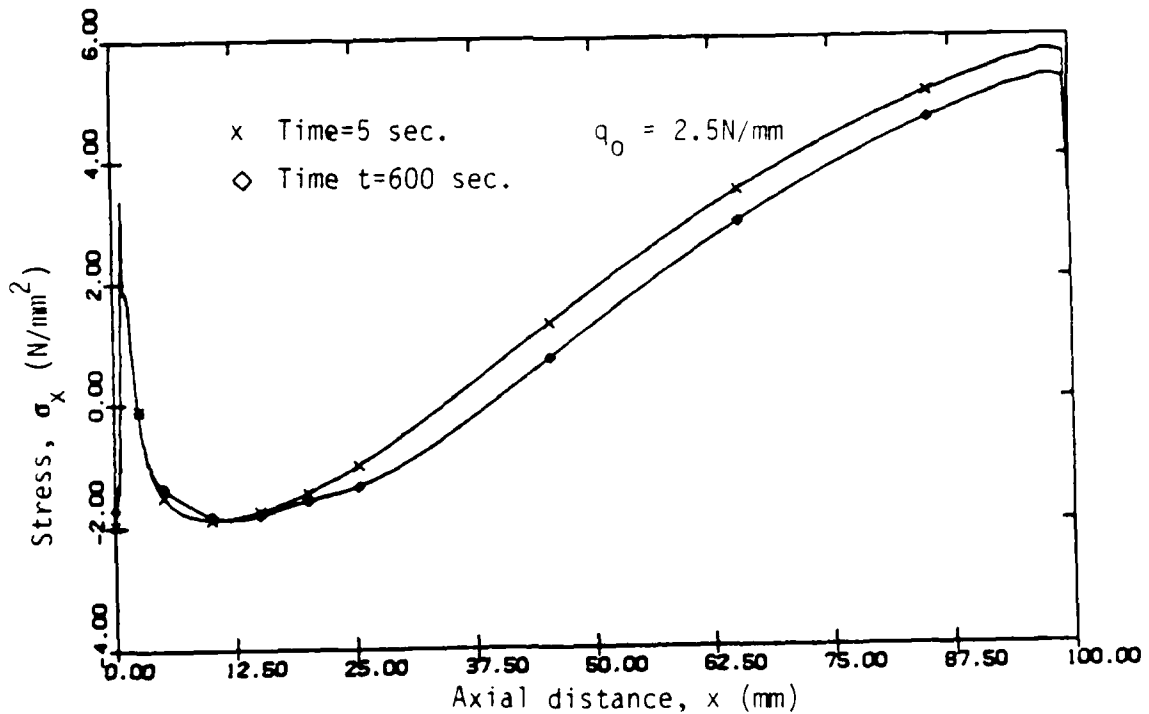
(b) Axial stress in the adhesive at y=5.01 mm

Fig. 9   Axial stresses in the adherend and the adhesive near the interface for transverse load q_o = 2.5 N/mm.

44
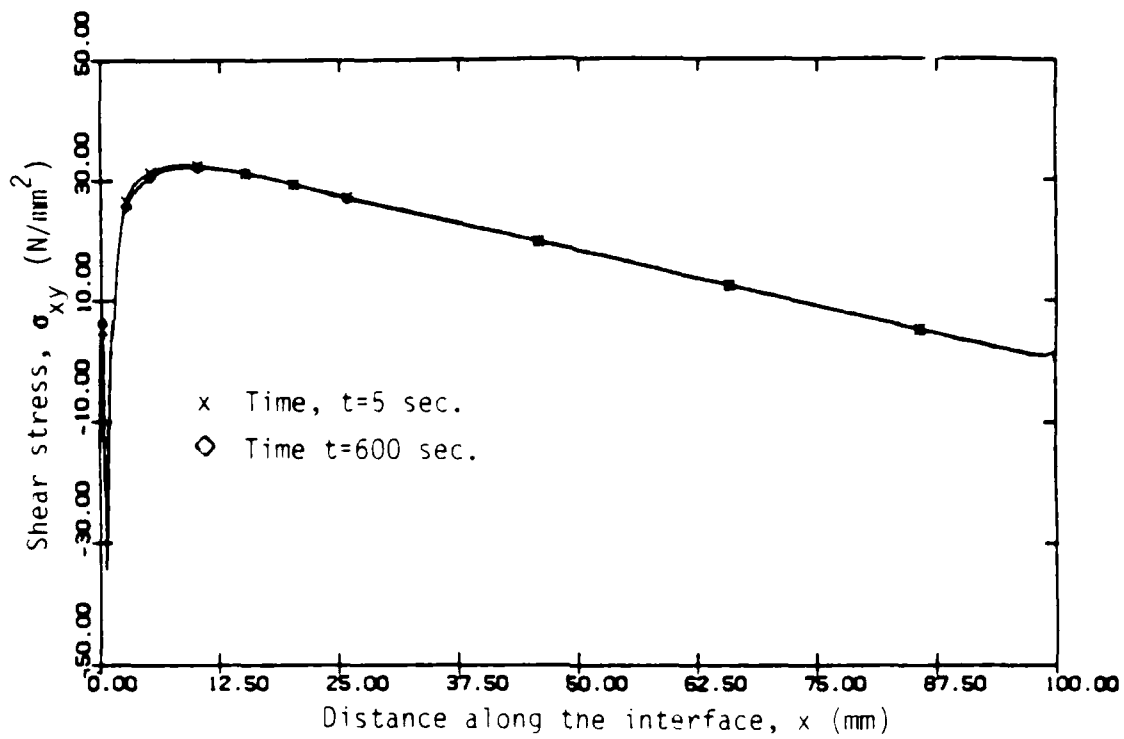
(a) Shear stress in aluminum at $y=4.96$ mm
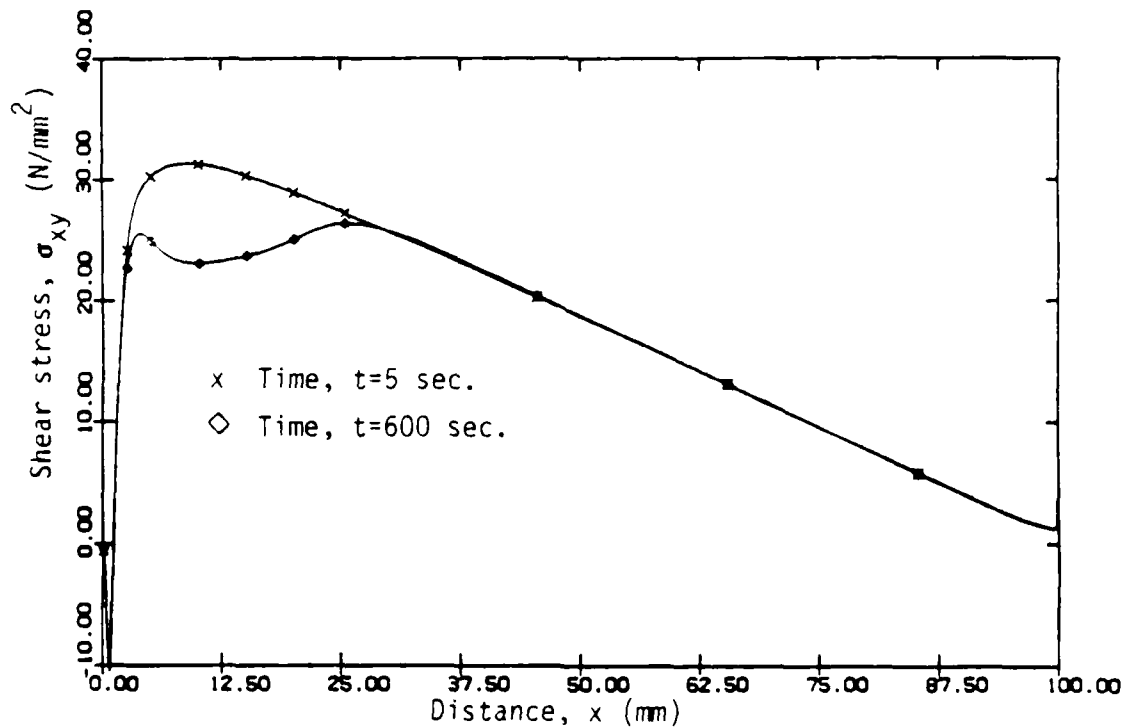
(b) Shear stress in adhesive at $y=5.01$ mm

Fig. 10 Variation of shear stresses in the adherend and adhesive near the interface for $q_0=2.5$ N/mm.
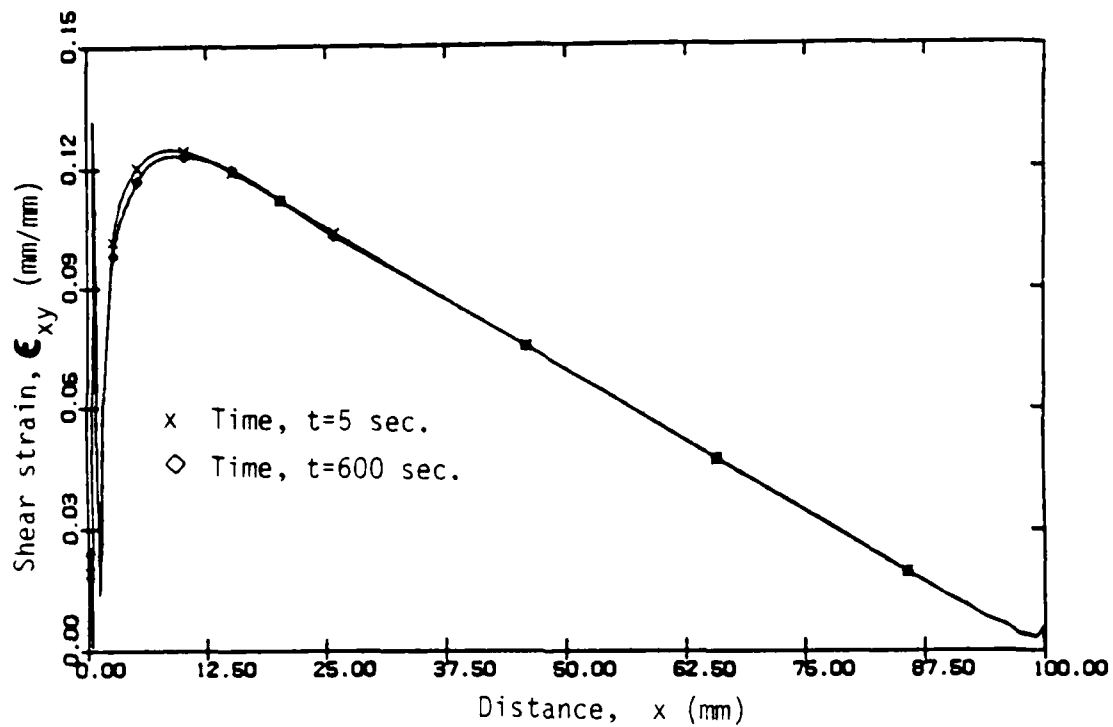
(a) Shear strain in aluminum at $y=4.96$ mm
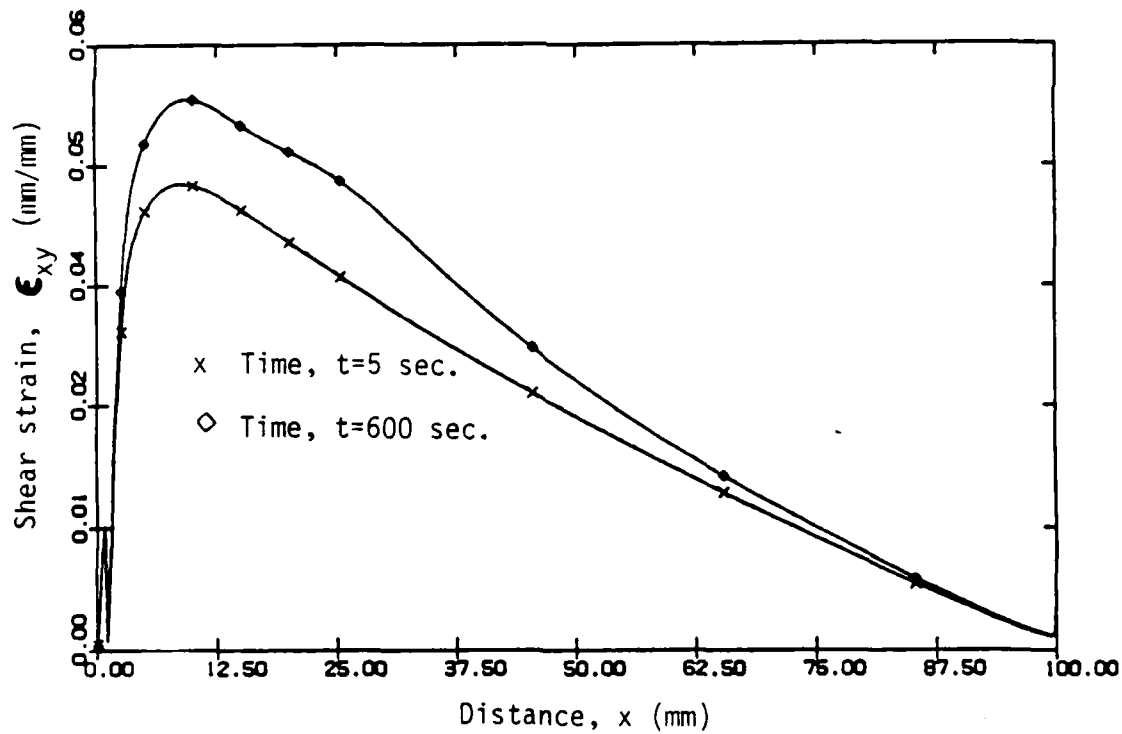
(b) Shear strain in the adhesive at $y=5.01$ mm

Fig. 11 Shear strain variation along the plate length in the
adherend and adhesive for transverse load, $q_o=2.5$ N/mm.
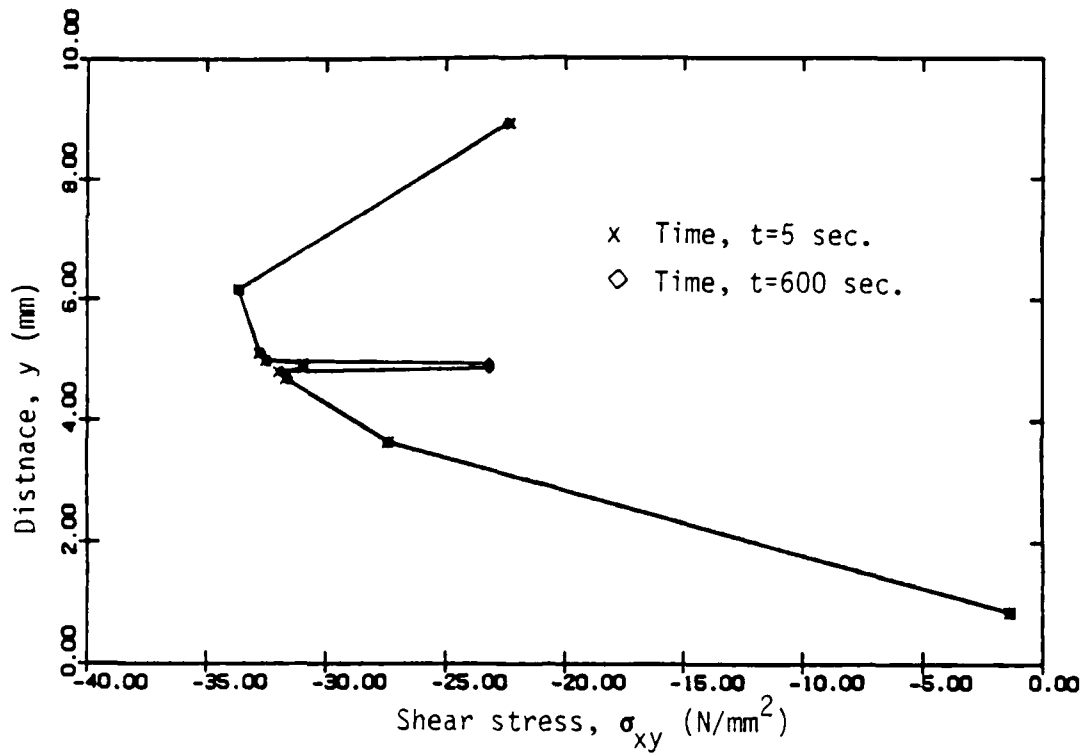
(a) Shear stress through thickness at x=13 mm
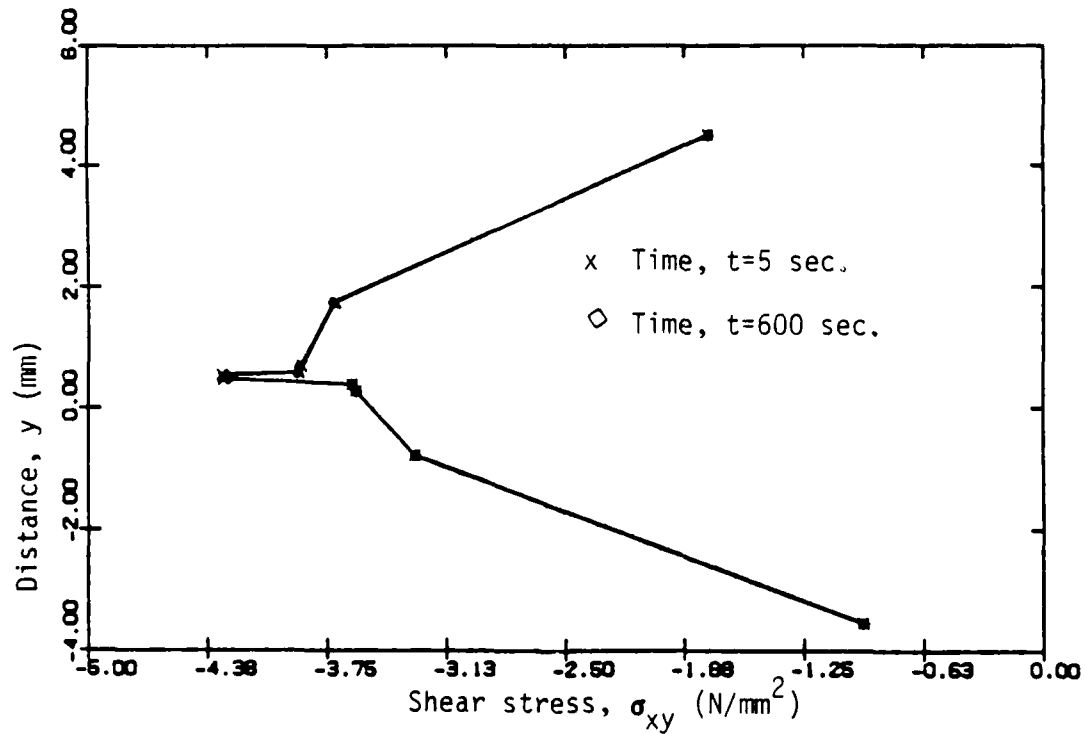
(b) Shear stress through thickness at x=89 mm

Fig. 12   Variation of shear stress through the thickness of the
bonded plate at x=13 and 89 mm for q_o = 2.5 N/mm.
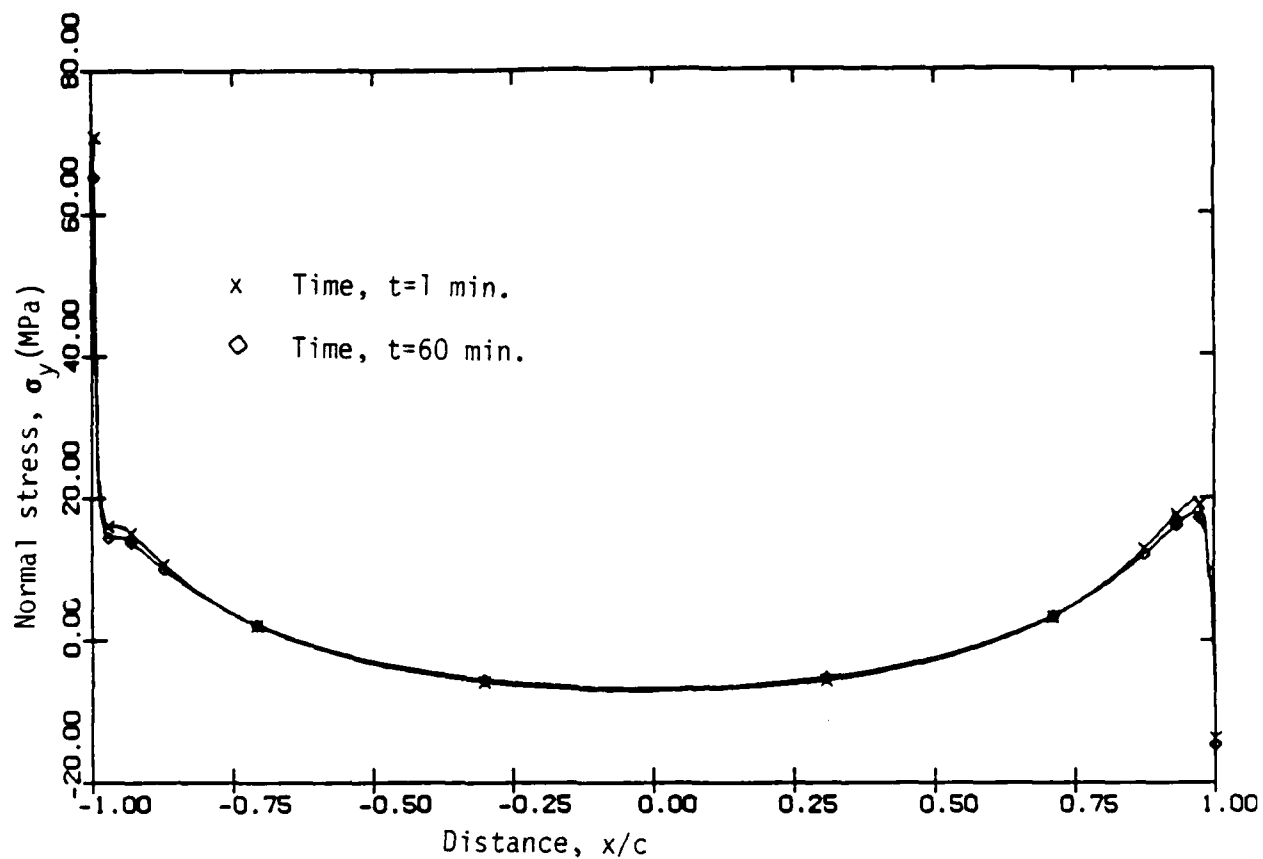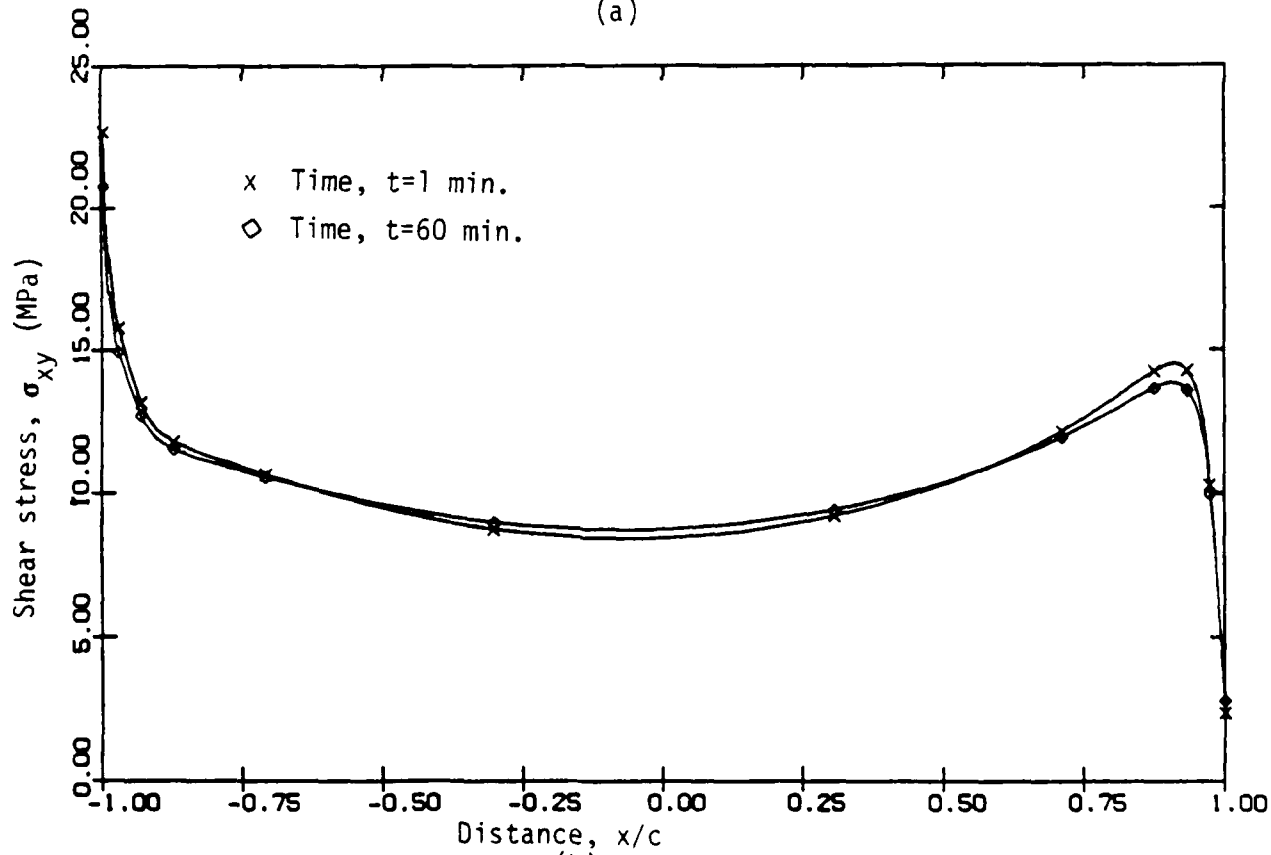
Fig. 13   Linear   viscoelastic plane strain analysis of a model joint
(variation of shear and peel stresses along theinterface).

48
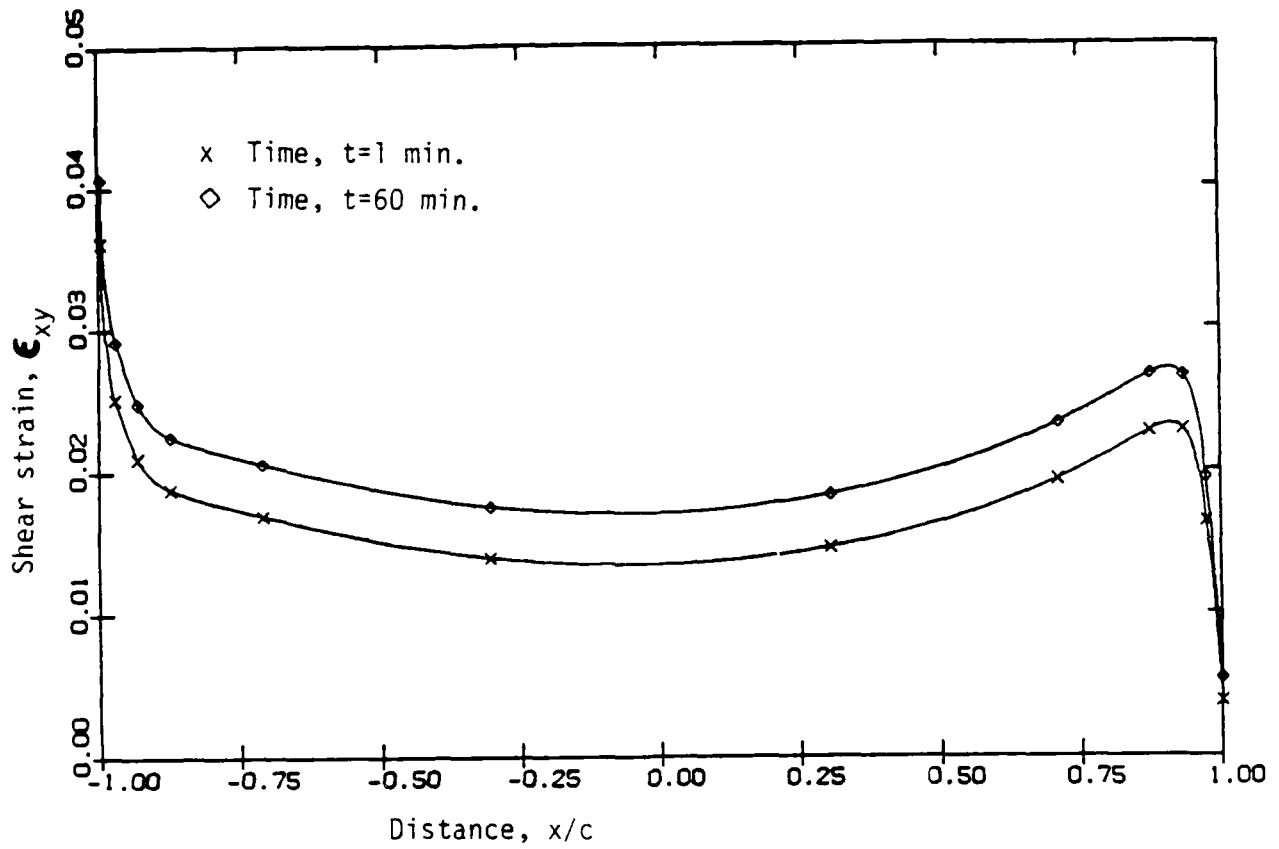
Fig. 14 Linear viscoelastic plane strain analysis of a model joint
(variation of the shear strain along the interface).
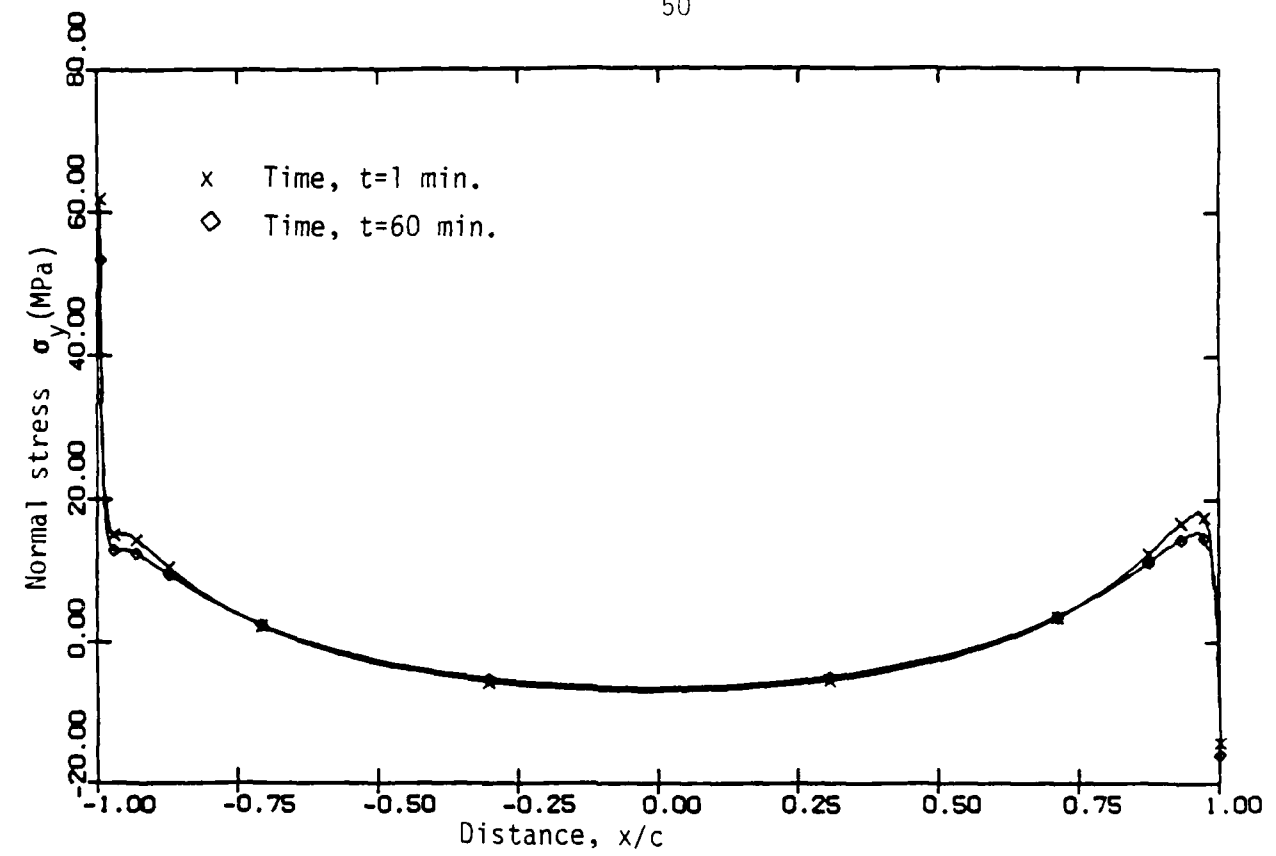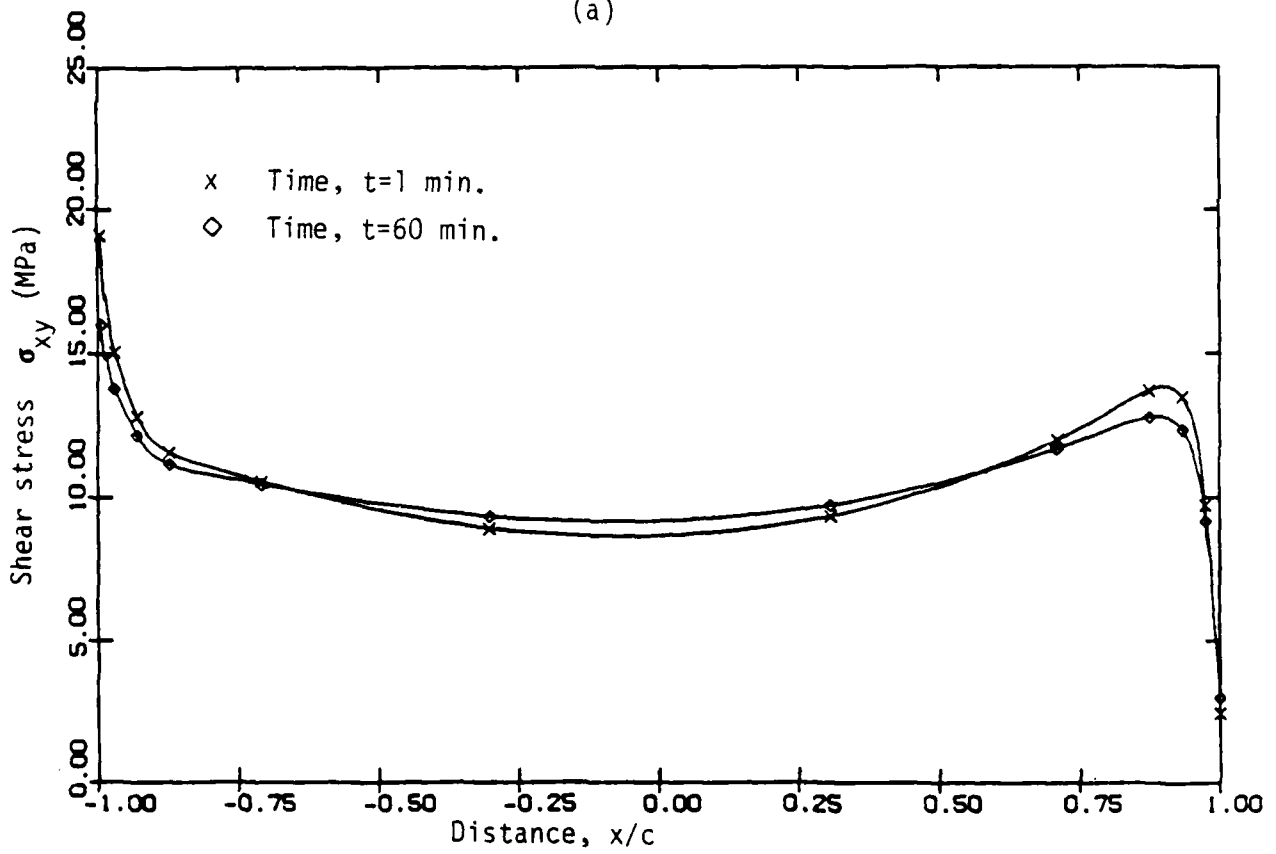
Fig. 15 Nonlinear viscoelastic analysis of a model joint (variation of normal and shear stresses at the interface).
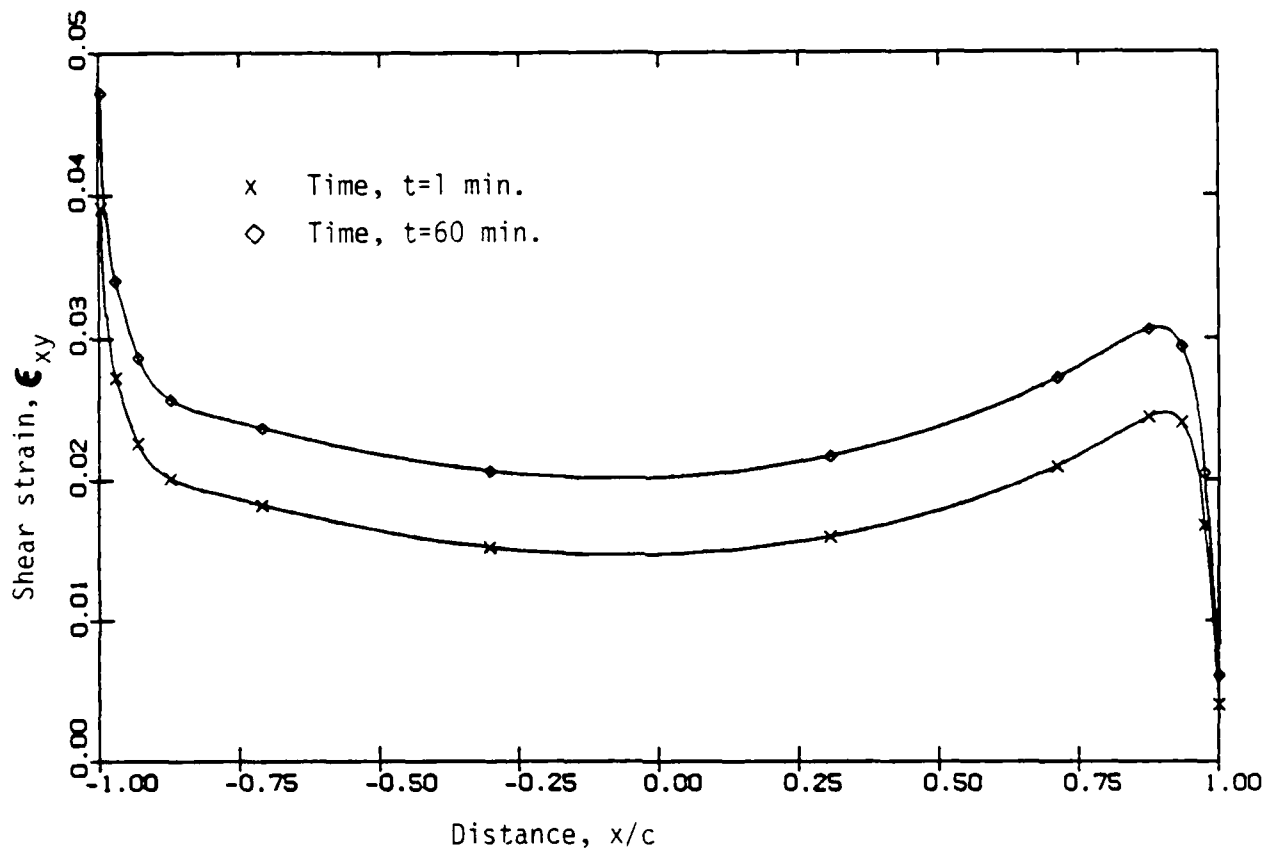
Fig. 16 Nonlinear viscoelastic analysis of a model joint (variation of shear strain along the interface).

117.475 mm

3.175 mm

107.95 mm

19.177 mm

6.35 mm
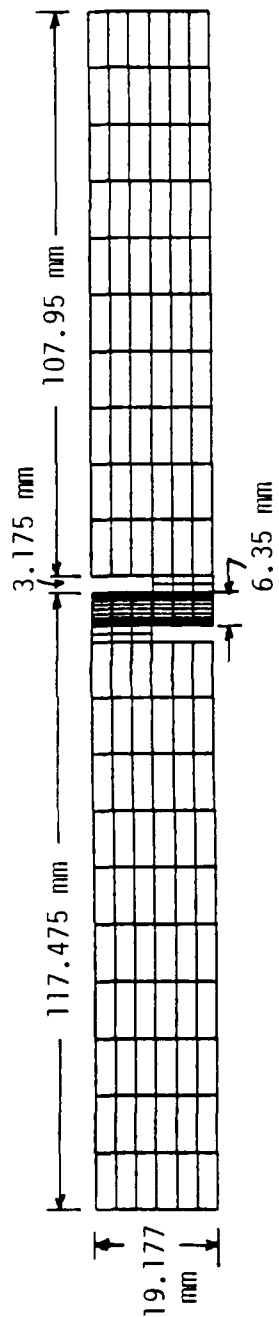
Thickness of the adhesive layer = 0.127 mm

Fig. 17 The geometry and finite element mesh used for the thick adherend lap shear specimen (see Fig. 2 for the boundary conditions).

52
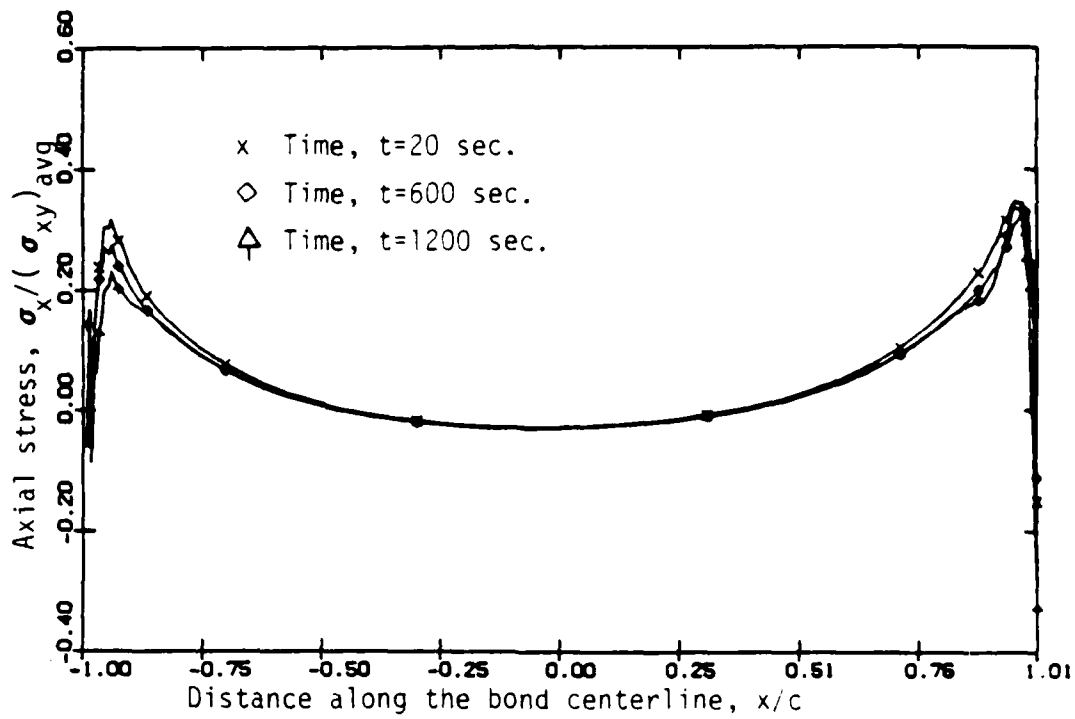
(a) Axial stress, $\sigma_x/(\sigma_{xy})_{avg}$
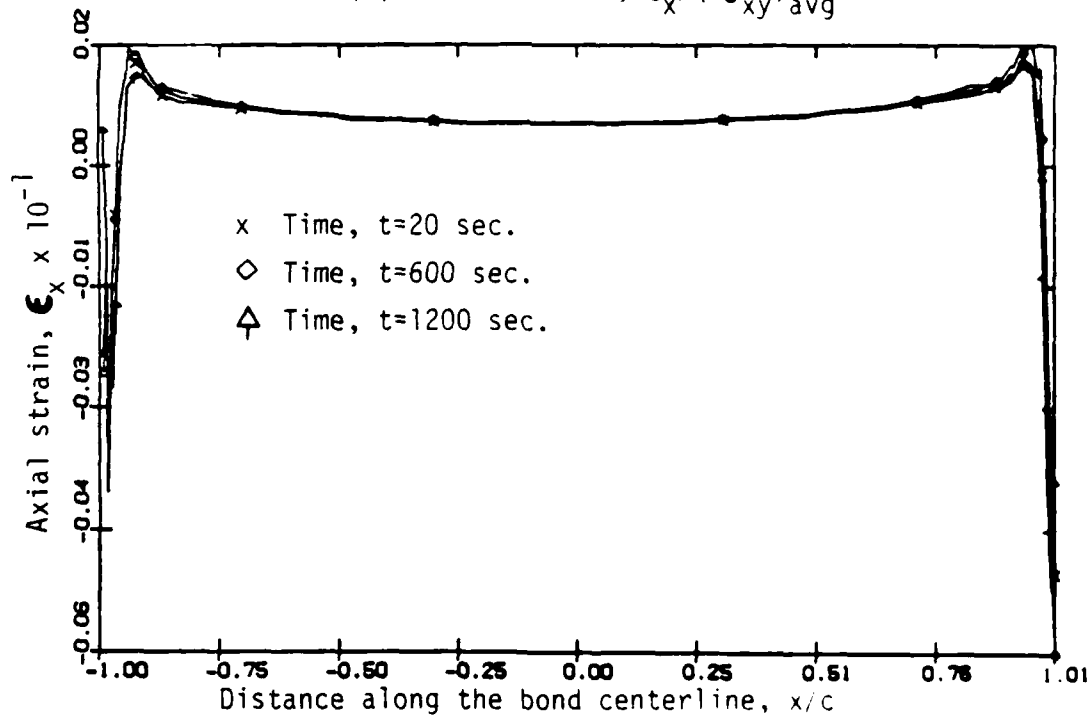
(b) Axial strain

Fig. 18 Variation of axial stress and strain along the bond center line for the thick adherend lap shear specimen problem.
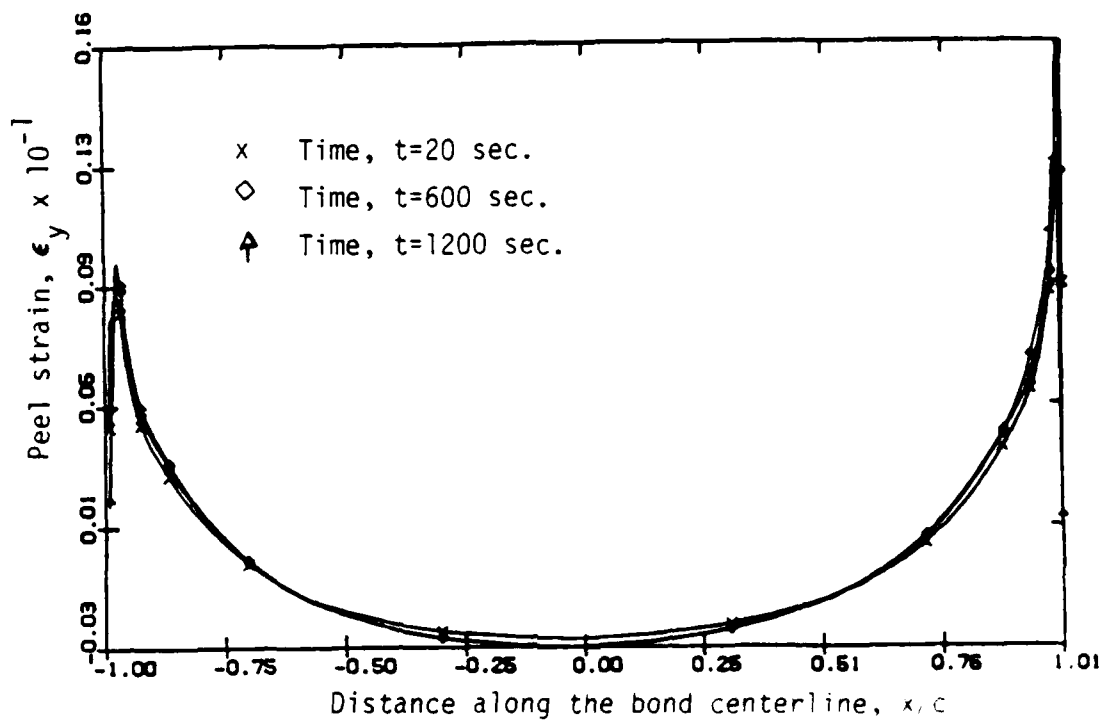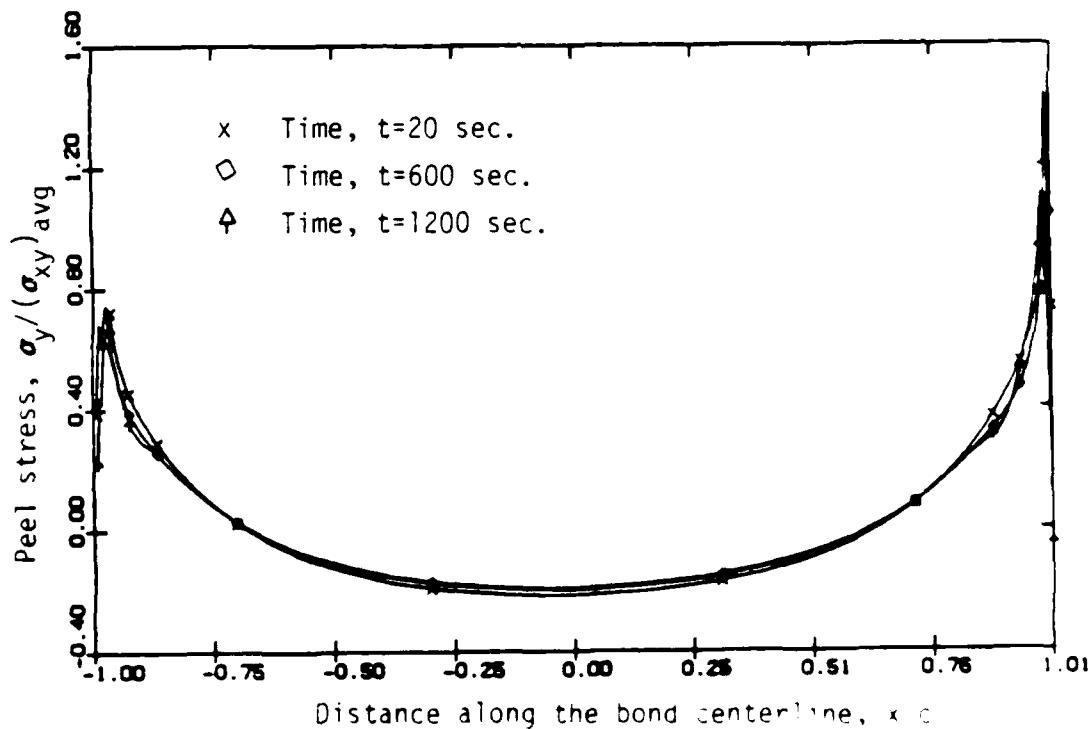
Fig. 19 Variation of peel strain and stress along the bond center line for the thick adherend lap shear specimen.
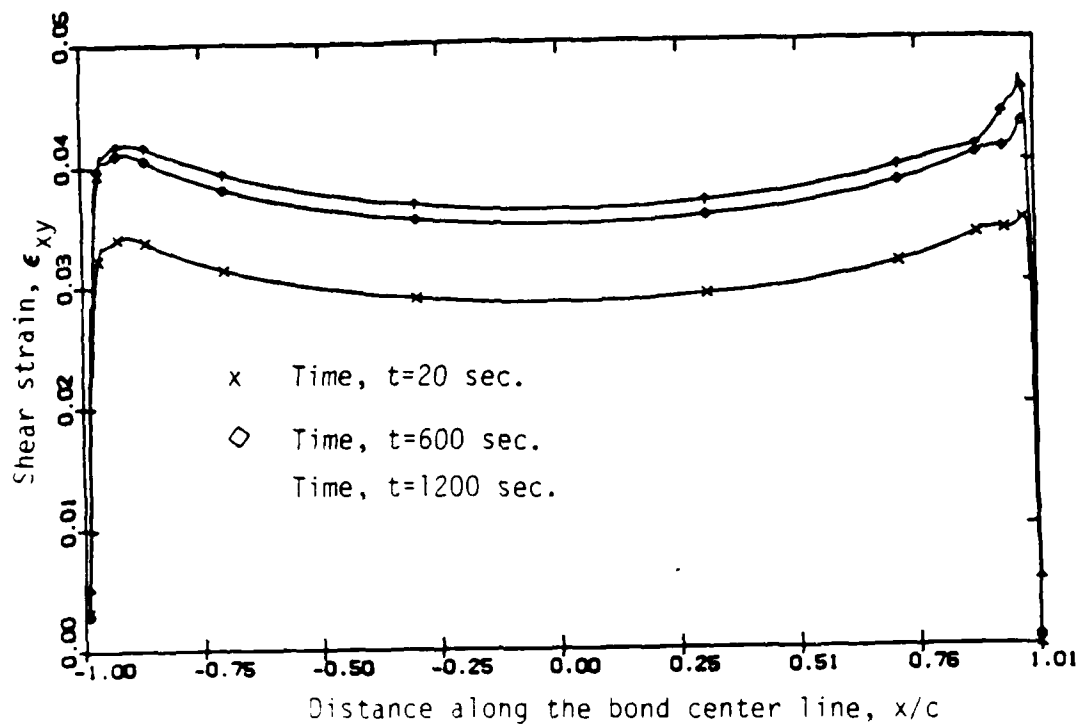
(a) Shear strain
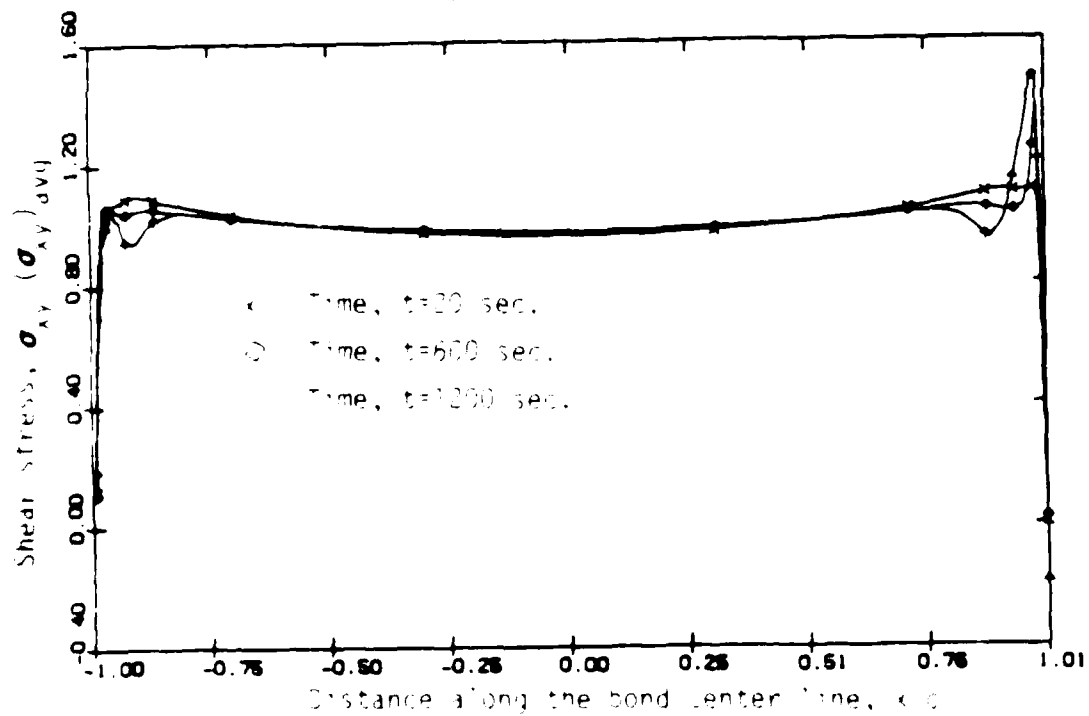
(b) Shear stress

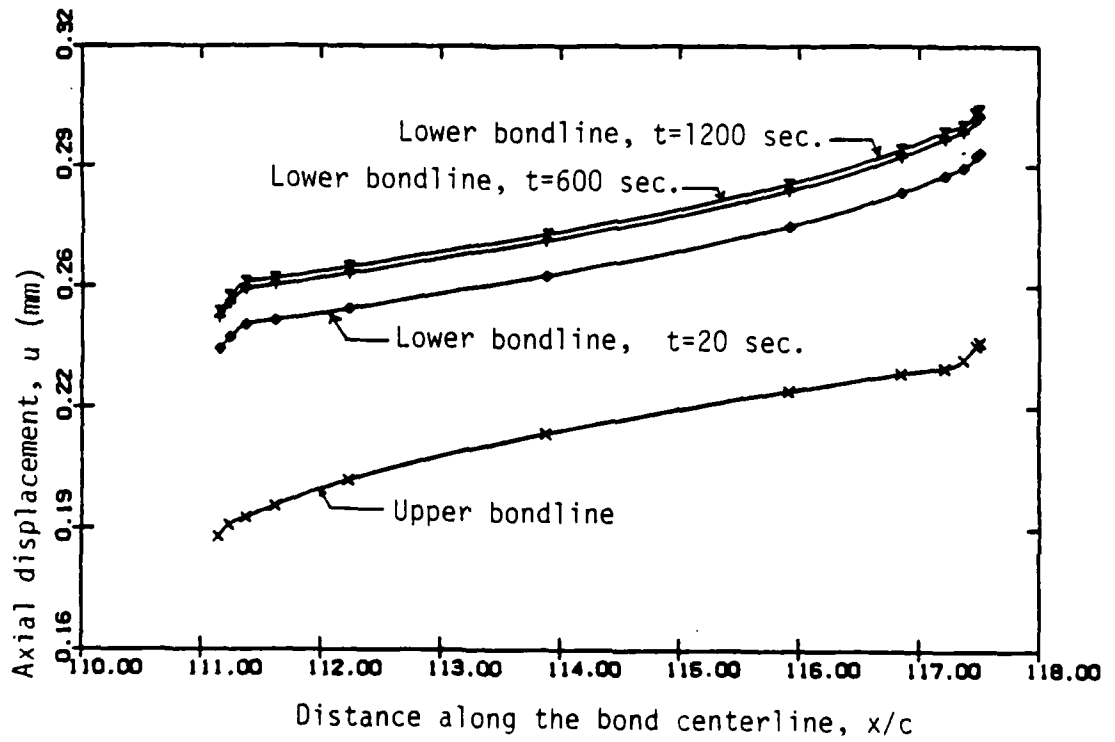Fig. 20 Variation of shear strain and stress along the bond center line for the thick adherend lap shear specimen.

Fig. 21 Variation of the axial displacement with the bond centerline
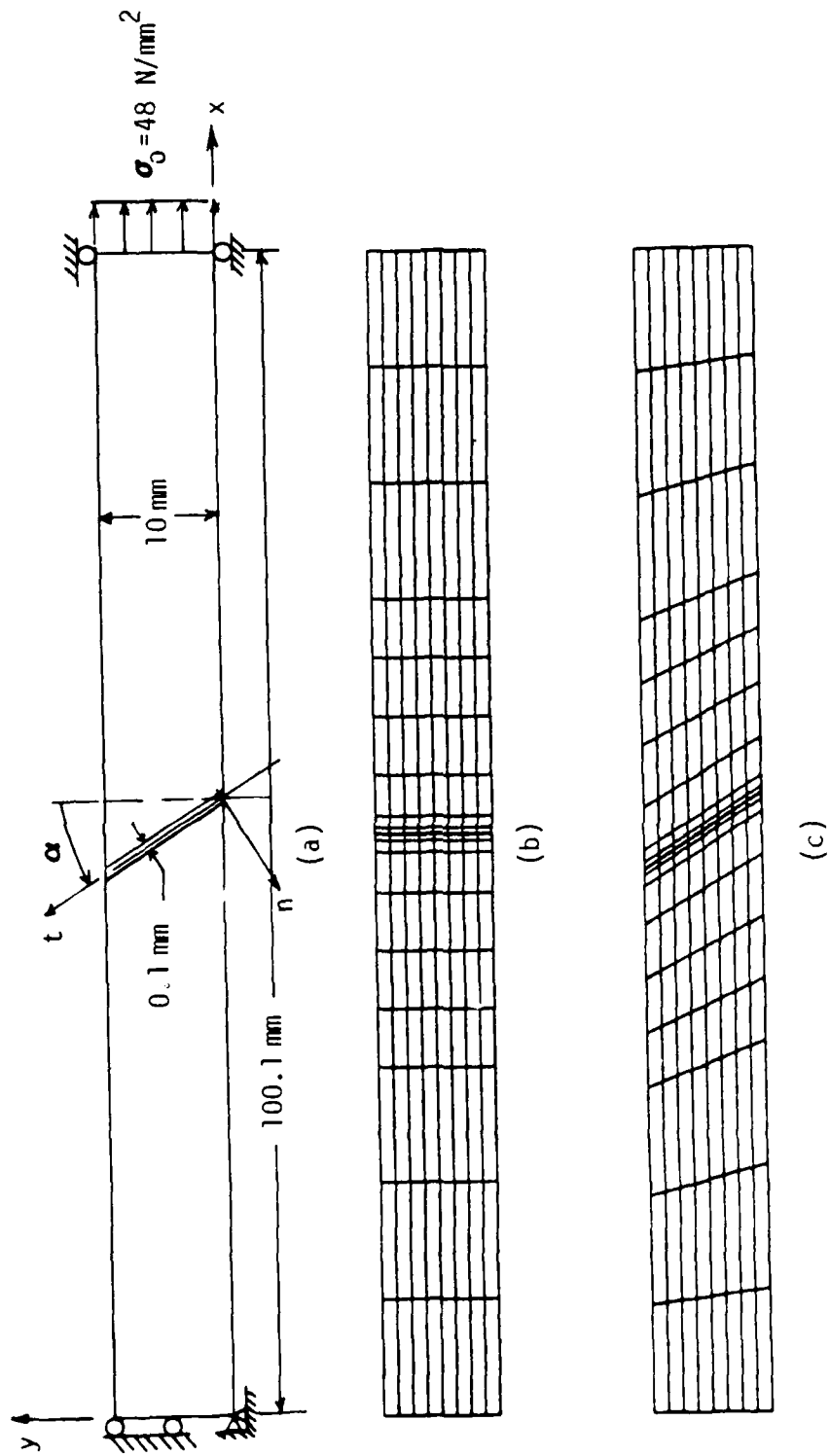for the thick adherend lap shear specimen.

Fig. 22 Geometry, boundary conditions, loading and finite element mesh used for the analysis of general scarf joint.
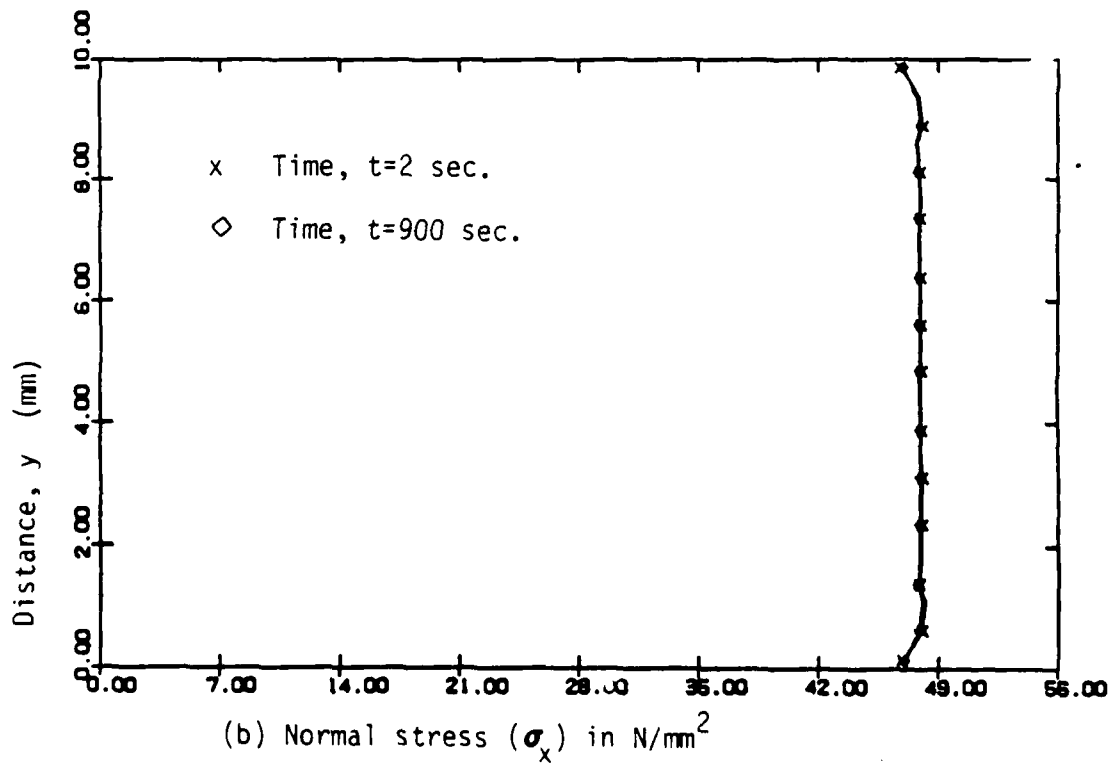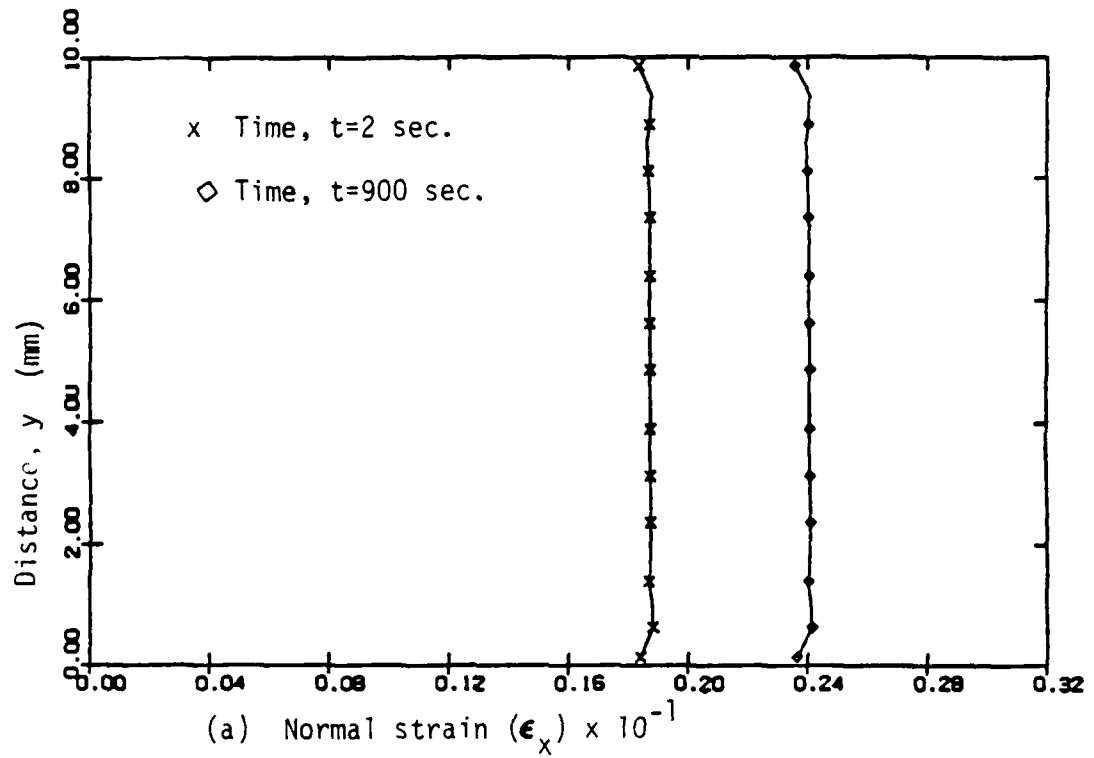
(a) Normal strain $(\epsilon_x) \times 10^{-1}$

(b) Normal stress (σ_x) in N/mm^2

Fig. 23 Variation of normal strain and stress along the adhesive
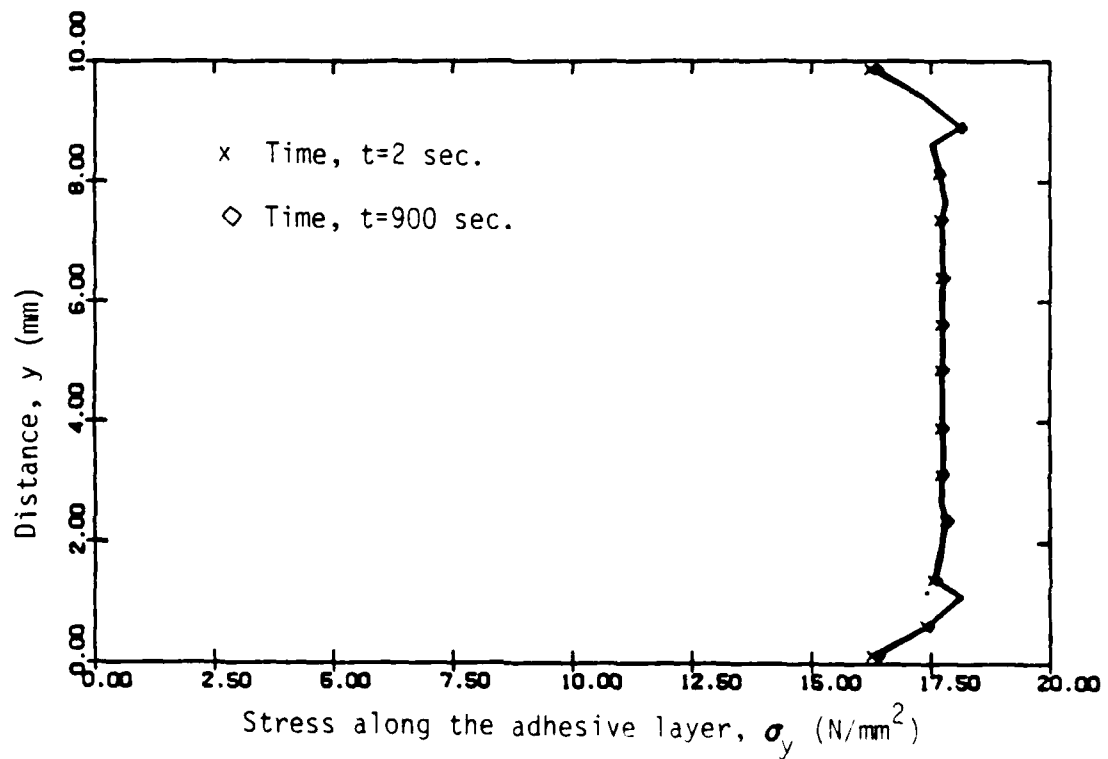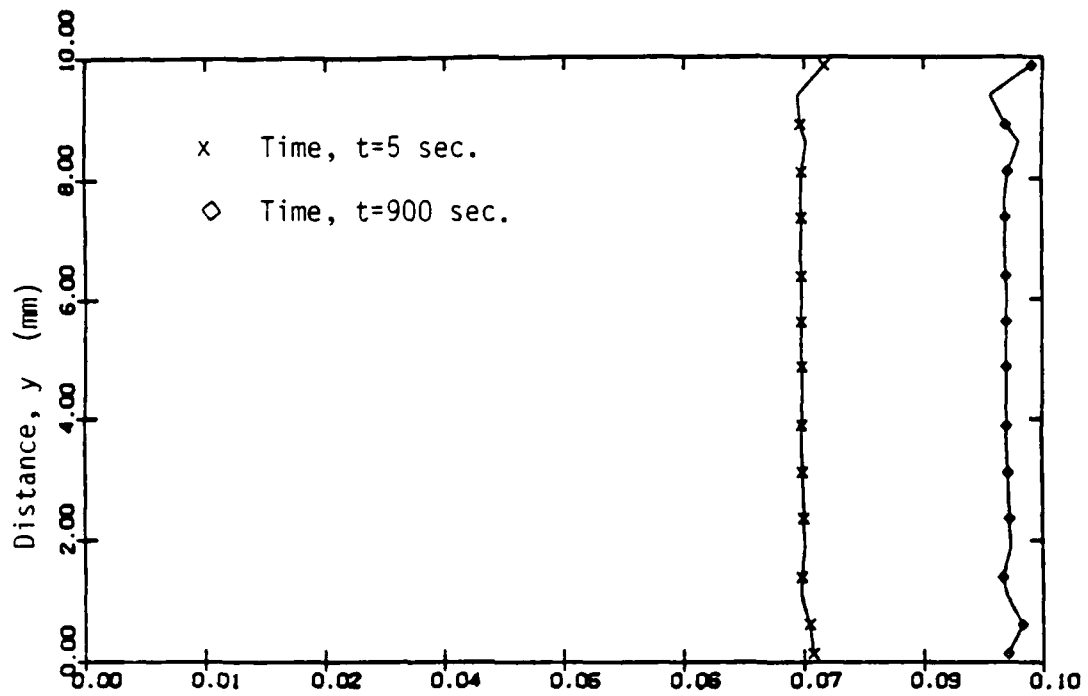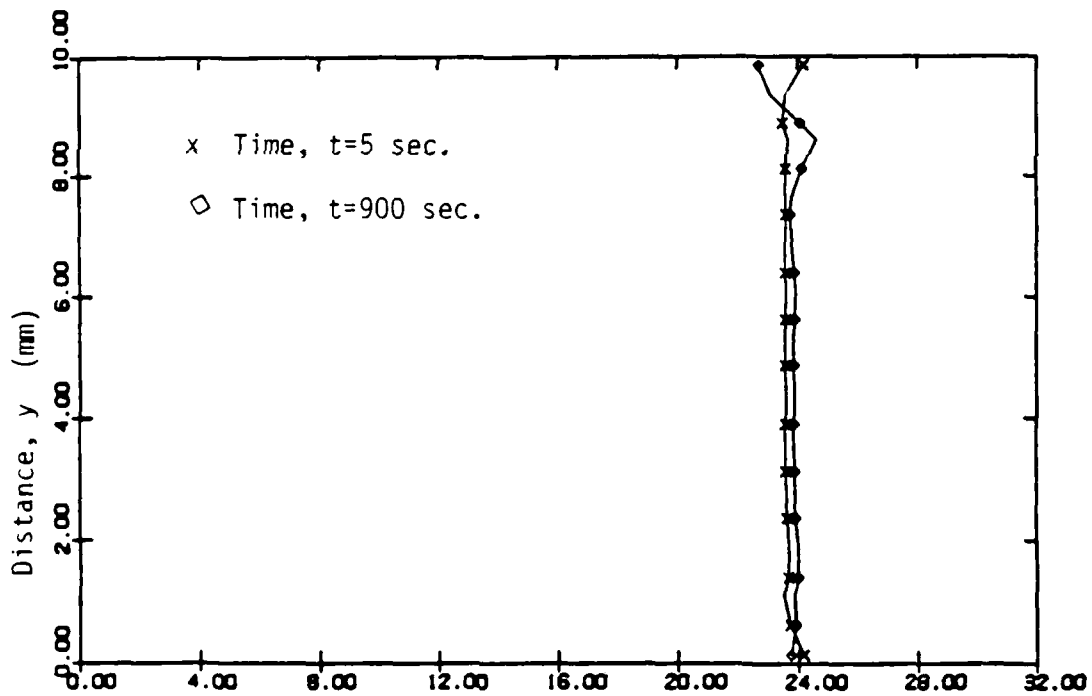layer for the butt joint ($\alpha = 0°$).

Fig. 24   Transverse stress in the adhesive layer (along the centerline of the adhesive layer) in the butt joint.

(a) Normal strain in the adhesive, $\epsilon_n \times 10^{-1}$

(b) Normal stress in the adhesive, σ_n (N/mm^2)

Fig. 25 Variation of the normal strain and stress along the depth of the scarf joint (for $\lambda = 45°$; see Fig. 22 for the angle and normal direction).

(a)   Shear strain ϵ_{nt} along the adhesive layer

(b)   Shear stress σ_{nt} (N/mm^2) along the adhesive layer
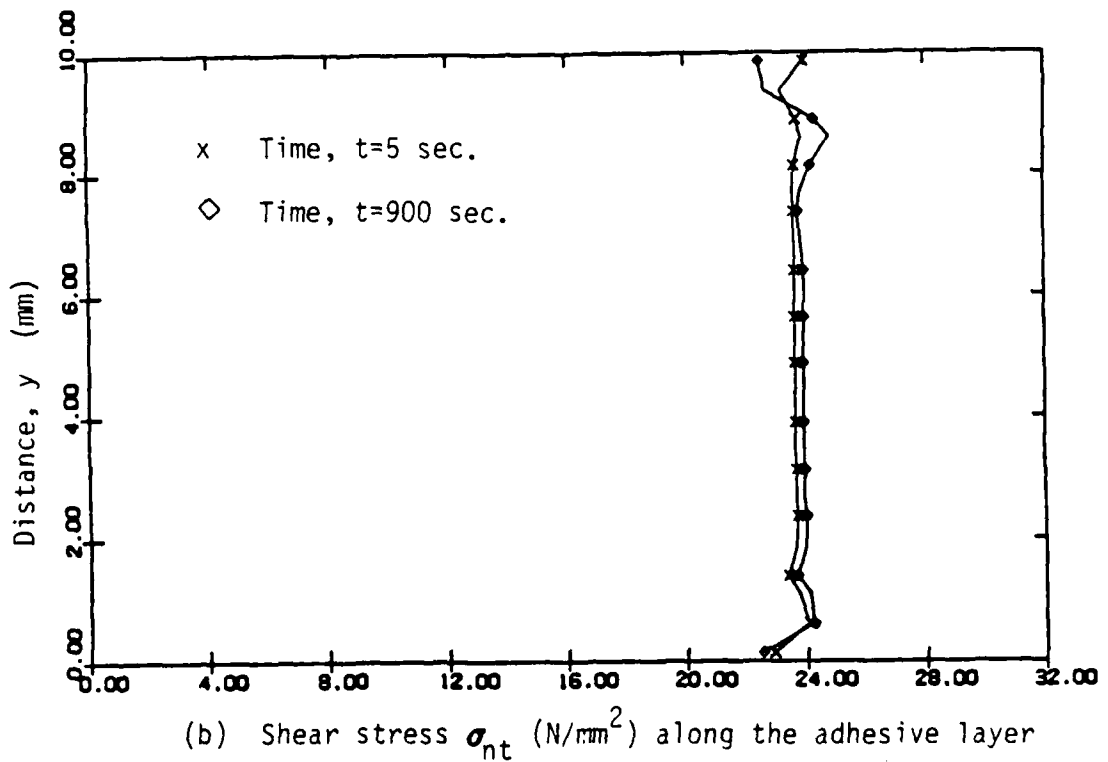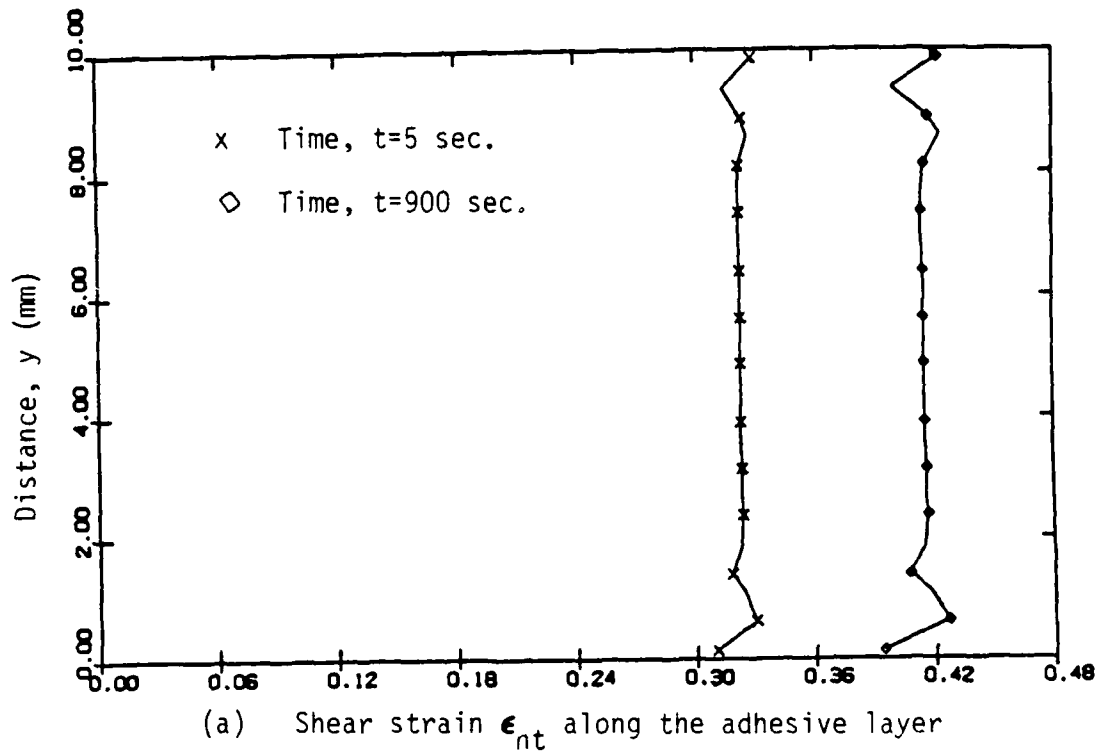
Fig. 26   Variation of shear strain and stress along the adhesive
for the scarf joint ($\alpha = 45°$, $\sigma_0 = 48N/mm^2$).

SECURITY CLASSIFICATION OF THIS PAGE *(When Data Entered)*

REPORT DOCUMENTATION PAGE		READ INSTRUCTIONS BEFORE COMPLETING FORM
1. REPORT NUMBER	2. GOVT ACCESSION NO.	3. RECIPIENT'S CATALOG NUMBER
4. TITLE *(and Subtitle)* NONLINEAR VISCOELASTIC ANALYSIS OF ADHESIVELY BONDED JOINTS		5. TYPE OF REPORT & PERIOD COVERED Interim
		6. PERFORMING ORG. REPORT NUMBER VPI-E-86.28/CAS/ESM-86-4
7. AUTHOR(s) S. ROY and J. N. REDDY		8. CONTRACT OR GRANT NUMBER(s) N00014-82-K-0185
9. PERFORMING ORGANIZATION NAME AND ADDRESS Virginia Polytechnic Institute and State University Blacksburg, Virginia 24061		10. PROGRAM ELEMENT, PROJECT, TASK AREA & WORK UNIT NUMBERS NR-039-229/8-12-83 (431)
11. CONTROLLING OFFICE NAME AND ADDRESS Office of Naval Research Mechanics Division (Code 431) 800 N. Quincy St., Arlington, VA 22217		12. REPORT DATE November 1986
		13. NUMBER OF PAGES 63
14. MONITORING AGENCY NAME & ADDRESS *(if different from Controlling Office)*		15. SECURITY CLASS. *(of this report)* UNCLASSIFIED
		15a. DECLASSIFICATION/DOWNGRADING SCHEDULE

16. DISTRIBUTION STATEMENT *(of this Report)*

This document has been approved for public release and sale; distribution unlimited.

17. DISTRIBUTION STATEMENT *(of the abstract entered in Block 20, if different from Report)*

18. SUPPLEMENTARY NOTES

19. KEY WORDS *(Continue on reverse side if necessary and identify by block number)*

Adhesive bonding, finite elements, incremental formulation, geometric nonlinearity, nonlinear viscoelastic model, updated Lagrangian formulation, numerical examples.

20. ABSTRACT *(Continue on reverse side if necessary and identify by block number)*

The report deals with the development of a numerical/computational procedure based on the updated Lagrangian formulation of two-dimensional continuum theory and nonlinear viscoelastic model of Schapery for the stress and deformation analysis of adhesively bonded joints. Schapery's uniaxial, single-integral law for nonlinear viscoelastic behavior is modified for two dimensions and included in the incremental, updated Lagrangian formulation that includes geometric nonlinear effects. The finite element method is used to solve the resulting differential equations, and a number of validation and sample problem results are presented.

DD $_{1\ JAN\ 73}^{FORM}$ **1473**   EDITION OF 1 NOV 65 IS OBSOLETE   UNCLASSIFIED

SECURITY CLASSIFICATION OF THIS PAGE *(When Data Entered)*